WRDC-TR-90-4078

AD-A236 092


# LOW-VELOCITY IMPACT TESTING OF THERMOPLASTIC AND THERMOSET MATRIX COMPOSITE MATERIALS

FINAL REPORT FOR PERIOD JANUARY 1985-JANUARY 1988

MARGARET F. PINNELL
STRUCTURAL MATERIALS BRANCH
NONMETALLIC MATERIALS DIVISION

PETER O. SJOBLOM
UNIVERSITY OF DAYTON RESEARCH INSTITUTE
300 COLLEGE PARK
DAYTON OHIO 45469-0001

DTIC
ELECTE
JUN 0 3 1991
S B D

NOVEMBER 1990

APPROVED FOR PUBLIC RELEASE--DISTRIBUTION UNLIMITED

MATERIALS LABRATORY
WRIGHT RESEARCH AND DEVELOPMENT CENTER
AIR FORCE SYSTEMS COMMAND
WRIGHT-PATTERSON AIR FORCE BASE OHIO 45433-6533

91-00898

91 5 30 059

# NOTICE

WHEN GOVERNMENT DRAWINGS, SPECIFICATIONS, OR OTHER DATA ARE USED FOR ANY PURPOSE OTHER THAN IN CONNECTION WITH A DEFINITELY GOVERNMENT-RELATED PROCUREMENT, THE UNITED STATES GOVERNMENT INCURS NO RESPONSIBILITY OR ANY OBLIGATION WHATSOEVER. THE FACT THAT THE GOVERNMENT MAY HAVE FORMULATED OR IN ANY WAY SUPPLIED THE SAID DRAWINGS, SPECIFICATIONS, OR OTHER DATA, IS NOT TO BE REGARDED BY IMPLICATION, OR OTHERWISE IN ANY MANNER CONSTRUED, AS LICENSING THE HOLDER, OR ANY OTHER PERSON OR CORPORATION; OR AS CONVEYING ANY RIGHTS OR PERMISSION TO MANUFACTURE, USE, OR SELL ANY PATENTED INVENTION THAT MAY IN ANY WAY BE RELATED THERETO.

THIS REPORT HAS BEEN REVIEWED BY THE OFFICE OF PUBLIC AFFAIRS (ASD/PA) AND IS RELEASABLE TO THE NATIONAL TECHNICAL INFORMATION SERVICE (NTIS). AT NTIS IT WILL BE AVAILABLE TO THE GENERAL PUBLIC INCLUDING FOREIGN NATIONS.

THIS TECHNICAL REPORT HAS BEEN REVIEWED AND IS APPROVED FOR PUBLICATION.

for MARGARET F. PINNELL, Mech Eng
Composites Group
Structural Materials Branch

CHARLES E. BROWNING, Chief
Structural Materials Branch
Nonmetallic Materials Division

FOR THE COMMANDER

MERRILL L. MINGES, Director
Nonmetallic Materials Division
Materials Laboratory

IF YOUR ADDRESS HAS CHANGED, IF YOU WISH TO BE REMOVED FROM OUR MAILING LIST, OR IF THE ADDRESSEE IS NO LONGER EMPLOYED BY YOUR ORGANIZATION PLEASE NOTIFY WRDC/MLBC, WRIGHT-PATTERSON AFB, OH 45433-6533 TO HELP MAINTAIN A CURRENT MAILING LIST.

COPIES OF THIS REPORT SHOULD NOT BE RETURNED UNLESS RETURN IS REQUIRED BY SECURITY CONSIDERATIONS, CONTRACTUAL OBLIGATIONS, OR NOTICE ON A SPECIFIC DOCUMENT.

# REPORT DOCUMENTATION PAGE

Form Approved
OMB No. 0704-0188

Public reporting burden for this collection of information is estimated to average 1 hour per response, including the time for reviewing instructions, searching existing data sources, gathering and maintaining the data needed, and completing and reviewing the collection of information. Send comments regarding this burden estimate or any other aspect of this collection of information, including suggestions for reducing this burden, to Washington Headquarters Services, Directorate for information Operations and Reports, 1215 Jefferson Davis Highway, Suite 1204, Arlington, VA 22202-4302, and to the Office of Management and Budget, Paperwork Reduction Project (0704-0188), Washington, DC 20503.

| 1. AGENCY USE ONLY (Leave blank) | 2. REPORT DATE | 3. REPORT TYPE AND DATES COVERED |
|---|---|---|
| | 9 Nov 90 | Final/Jan 85-Jan 88 |

**4. TITLE AND SUBTITLE**
Low-Velocity Impact Testing of Thermoplastic and Thermoset Matrix Composite Materials

**5. FUNDING NUMBERS**
62102F
24190310

**6. AUTHOR(S)**
Pinnell, Margaret F.
Sjoblom, Peter O.

**7. PERFORMING ORGANIZATION NAME(S) AND ADDRESS(ES)**
WRDC/MLBC (Tobey Cordell, 255-9609)
Wright-Patterson AFB OH 45433-6533

**8. PERFORMING ORGANIZATION REPORT NUMBER**
WRDC-TR-90-4078

**9. SPONSORING/MONITORING AGENCY NAME(S) AND ADDRESS(ES)**
N/A

**10. SPONSORING/MONITORING AGENCY REPORT NUMBER**
N/A

**11. SUPPLEMENTARY NOTES**
N/A

**12a. DISTRIBUTION/AVAILABILITY STATEMENT**
Approved for public release; distribution is unlimited.

**12b. DISTRIBUTION CODE**
N/A

**13. ABSTRACT** *(Maximum 200 words)*

The effects of boundary conditions, specimen thickness, indenter nose diameter, impact velocity and target material on the damage initiation load and mode of failure during low-velocity impact of composite materials are studied. A mathematical model is presented which theoretically predicts the effects of the various parameters on the damage initiation force. In addition, a comparison of the static indentation versus low-velocity impact results is made in an effort to prove that low-velocity impact can be sufficiently modelled using statically based theories. Experimental data indicated that the mathematical model predicts the effect of material thickness on damage initiation force very well. Data obtained from static indentation and low-velocity impact were found to be comparable. Some differences were noted in the impact failure modes of the two materials tested.

**14. SUBJECT TERMS**
Impact, Low-Velocity, Advanced Composites, Toughness, Thermoplastic, Thermoset, Damage Tolerance, Damage Resistance.

**15. NUMBER OF PAGES**
46

**16. PRICE CODE**

| 17. SECURITY CLASSIFICATION OF REPORT | 18. SECURITY CLASSIFICATION OF THIS PAGE | 19. SECURITY CLASSIFICATION OF ABSTRACT | 20. LIMITATION OF ABSTRACT |
|---|---|---|---|
| UNCLASSIFIED | UNCLASSIFIED | UNCLASSIFIED | |

# ACKNOWLEDGMENTS

The Authors wish to thank the following University of Dayton personnel: Mr. Ron Cornwell, Mr. John Camping, and Dr. Ran Kim for their contributions to this research effort, Dr. Al Berens for his help with the statistical analysis of the data, and Ms. Anita Cochran for her help editing the manuscript.


Accession For
NTIS GRA&I ☑
DTIC TAB ☐
Unannounced ☐
Justification
By
Distribution/
Availability Codes
Dist | Avail and/or Special
A-1

# TABLE OF CONTENTS

# LIST OF FIGURES

# LIST OF TABLES

# SECTION 1. INTRODUCTION

The barely visible, extensive damage associated with low-velocity impacts on polymer matrix composites is a major concern to the designers and users of composites in aircraft. The potential threat of the hidden damage resulting from low-velocity impacts serves as motivation to gain a better understanding of the governing parameters associated with impact. Of particular interest to the aircraft designer are the relationships of material properties, material thickness, size of impacter, size of target, and impact velocity to the ability of the composite structure to absorb energy, the impact load required to initiate damage of the part, and the types of failure mechanisms occurring within the composite. The purpose of this in-house research effort was to gain a better understanding of low-velocity impact and to generate a substantial low-velocity impact database for two baseline composite materials using a pendulum-type test setup. The study began with a review of previous work done in the area of impact of composite materials. The theories which evolved from these prior research efforts were used to guide the selection of the parameters to be studied. An experimental approach was taken to determine the relationship of each parameter to the ability of the composite to absorb energy, the impact load required to initiate damage, and the types of failures occurring within the composite. An innovative pendulum-type test method was used to carry out the necessary experimentation.

The investigation was divided into three phases. In Phase 1, the effect of material thickness and specimen support size on the damage initiation force was investigated. The test matrix for this phase is given in Table 1.1. In Phase 2, the effect of indenter nose diameter on damage initiation force was studied. The test matrix for this phase is shown in Table 1.2. In Phase 3, the effect of impact velocity on damage initiation force was addressed. The test matrix for this phase is given in Table 1.3.

Impacted specimens from all three phases were subjected to ultrasonic C-scan examination and photomicrographs were taken of the impacted region to gain a better understanding of the damage area and the failure mechanisms in impacted composite materials.

This report describes the test technique used in this investigation. It also summarizes the large amount of data obtained from this investigation for the two baseline materials. Although the purpose of this research was not to compare the impact resistance of thermoset versus thermoplastic matrix systems, some observations were made concerning the very different behavior of these two material systems.

***Table 1.1 Phase 1 Test Matrix.***

| | |
|---|---|
| Materials: | Hercules AS-4/3502 |
| | ICI AS-4/APC-2 |
| Type Tests: | Static Indentation |
| | Low-Velocity Impact |
| Impacter Indenter Nose Dia: | 12.7 mm (0.5 in) |
| Specimen Support Dia.: | 25 mm (0.984 in) |
| | 50 mm (1.968 in) |
| | 75 mm (2.953 in) |
| | 100 mm (3.937 in) |
| Material Thickness: | 8 plies (~ 1.1 mm, 0.043 in) |
| | 16 plies (~ 2.2 mm, 0.087 in) |
| | 24 plies (~ 3.2 mm, 0.125 in) |
| | 32 plies (~ 4.3 mm, 0.169 in) |
| | *48 plies (~ 6.5 mm, 0.256 in) |
| | |
| * For AS-4/3502 only | |

***Table 1.2. Phase 2 Test Matrix.***

| | | |
|---|---|---|
| Materials: | Hercules AS-4/3502 | |
| | ICI AS-4/APC-2 | |
| Type Tests: | Low-Velocity Impact | |
| Impacter Indenter Nose Dia: | 6.35 mm | (0.25 in) |
| | 12.7 mm | (0.50 in) |
| | 25.4 mm | (1.00 in) |
| | 50.8 mm | (2.00 in) |
| Specimen Support Dia.: | 25 mm | (0.984 in) |
| | 50 mm | (1.968 in) |
| | 100 mm | (3.937 in) |
| Material Thickness: | 16 plies | (~ 2.2 mm, 0.087 in) |
| | 32 plies | (~4.3 mm, 0.169 in) |

***Table 1.3. Phase 3 Test Matrix.***

| | | |
|---|---|---|
| Materials: | Hercules AS-4/3501-6 | |
| | ICI AS-4/APC-2 | |
| Type Tests: | Low-Velocity Impact | |
| Impacter Indenter Nose Dia: | 12.7 mm | (0.50 in) |
| Specimen Support Dia: | 50 mm | (1.968 in) |
| | 100 mm | (3.937 in) |
| Material Thickness: | 16 plies | (~.2.2 mm, 0.087 in) |
| | 32 plies | (~ 4.3 mm, 0.169 in) |
| Velocity at Impact: | 1.3 m/s | (4.2 ft/s) |
| | 2.0 m/s | (6.6 ft/s) |
| | 3.0 m/s | (9.8 ft/s) |
| | 4.0 m/s | (13 ft/s) |
| | 5.0 m/s | (16 ft/s) |
| | | |

# SECTION 2. BACKGROUND

The subject of impact damage to composite materials is of critical concern in the aeronautical world today. Several classes of impact damage can be experienced by an aircraft. The most easily recognizable type of impact is that which a structure might incur during battle. Battle damage impact is associated with very high impact velocities and generally results in complete penetration of the foreign object through the structure. Another type of impact which has troubled the designers of fighter canopies for years is the type of impact that occurs during flight operations. This type of impact includes bird strikes, hail, and runway debris, and generally results in significant and visible damage to composite structures. Of growing concern to the design engineer is low-velocity (i.e. < 6 m/s ) impact which occurs during fabrication, maintenance, and operation of an aircraft. The dropping of a tool or a tool box onto a composite wing skin and the improper loading of equipment onto an airplane are two instances where this type of impact might occur. A good overview of this problem is presented in [1]. Damage resulting from low-velocity impacts is usually not visible from the impacted side of the structure; however, significant delamination and back face damage may be present.

Of the types of impacts mentioned above, low-velocity impact is considered most threatening to composite structures, because the nature of the damage is such that it cannot be seen from the impacted side of the structure. Such damage might easily go undetected during routine visual inspection and thus damaged parts may be put into service. The fact that low-velocity impacts can result in extensive damage extending well beyond the immediate impacter contact area adds to the deceptive nature of the damage associated with low-velocity impact. Furthermore, it has been shown that such damage produces a drastic reduction in residual compression strength of a composite structure. For this reason a greater understanding of the impact event, the resulting damage, and its effects on the residual compressive strength is needed.

## 2.1 The Impact Event

The impact event consists of relatively high contact forces acting on a small area over a short period of time. Local plastic and elastic deformation occurs in the structure as well as fiber and matrix fracture. If the structure is very thin and/or ductile, the plate may also undergo flexural deformation under the force of the impacter. This type of deformation leads to tensile and compressive forces on the lower and upper surface of the panel,

respectively. The damage resulting from this may be in the form of matrix cracking, delamination, and/or fiber fracture. Kitanka [2] points out that the matrix shear strength and the interlaminar fracture toughness are the material properties governing the initiation and propagation of these failures. Flexural deformation is the predominant mode for thin targets impacted at higher energy levels. Failure in this case is caused by tensile forces and initiates in the lowest ply in the form of fiber breakage or matrix cracking. This precipitates failure at the fiber matrix interface. The matrix crack then extends upward until the next interface is encountered. Here the crack is deflected upwards by the matrix crack to a higher ply, as seen in Figure 2.1 [3].

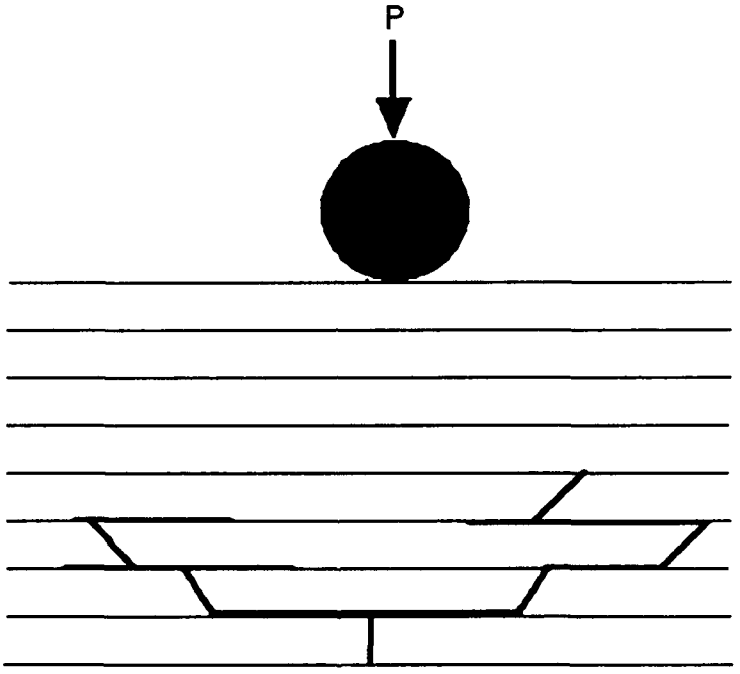


***Figure 2.1. Propagation of failure due to flexural deformation.***

Damage resulting from contact forces begins at the fiber matrix interface at the periphery of the area of contact on the uppermost ply. This failure is initiated by large shear stresses generated in the target around the impacter during contact. The initial failure propagates through the upper ply until it is deflected into a lower ply by matrix shear cracking. The shear stresses cause this cracking to extend in a conical fashion from the area of contact. As the area of impact increases during the penetration of the impacter, the location of the shear stresses changes. This results in a large number of shear cracks, as shown in Figure 2.2 [3].

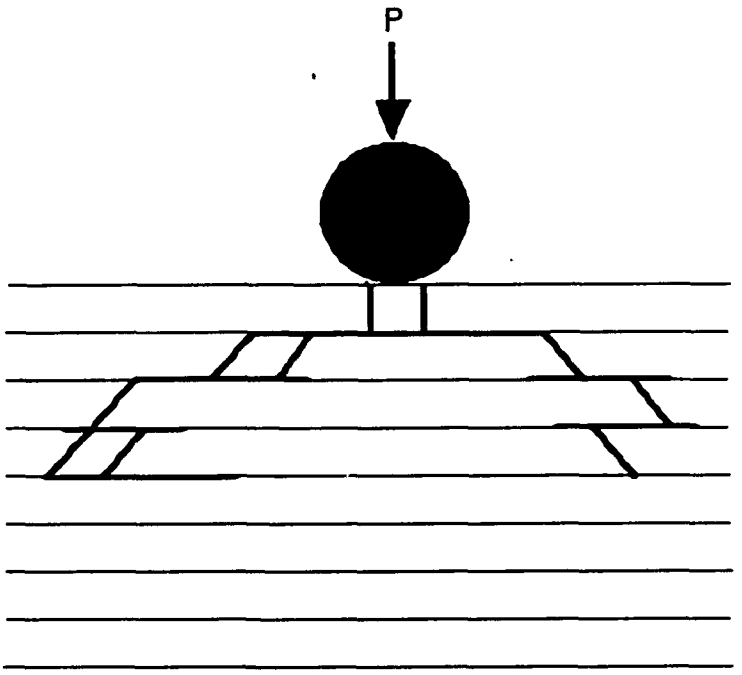


***Figure 2.2. Damage resulting from contact forces.***

## 2.2 Simple Theoretical Model

A very simple mathematical model to predict the damage initiation force of composite plates subjected to low-velocity impacts was presented in [4]. The purpose of this model is not to provide precise design type data, but rather to provide information concerning approximate trends of the damage initiation force as a function of various testing parameters. These parameters include the specimen thickness, specimen support size, and impacter size. Because this mathematical model served as the basis for determining the parameters studied in this investigation, an in-depth discussion of its derivation is included.

Derivation of the mathematical model involves several assumptions. The first assumption is that low-velocity impact includes only those impacts in which the impacter contact time is very long compared to the stress-wave propagation time (i.e., approximately static loading). The second assumption is that the target and impacter are linearly elastic. These two assumptions justify the application of the Hertz Contact Law to the low-velocity impact problem. The Hertz Contact Law is a force-deformation relation which describes the static compression of two isotropic, elastic bodies. It has been shown by Yang and Sun

that the Hertz Contact law can be applied to the case of a hard sphere being pressed into a composite plate [5]:

$$P = K_C \alpha^{3/2} \tag{2.1}$$

Where: $P$ = Impact Force
$K_C$ = Contact Stiffness
$\alpha$ = Depth of the Indentation

Considering the geometry of the impact the following relation is obtained in Figure 2.3:

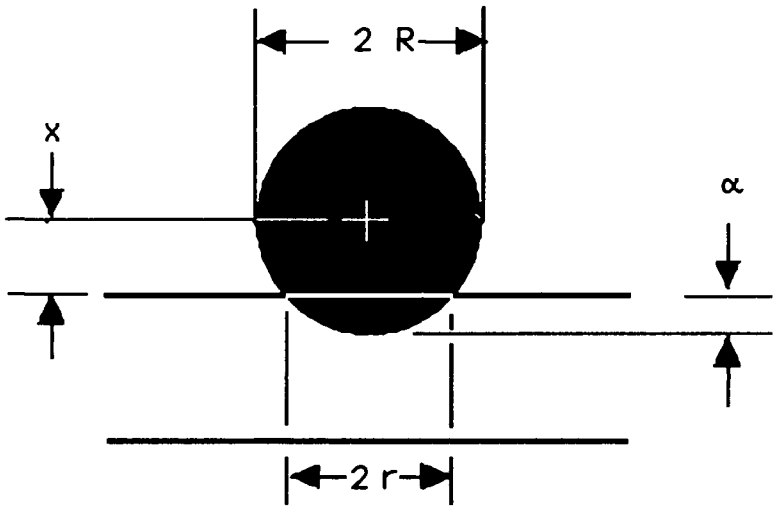


***Figure 2.3. Geometry of the impact.***

$$r = (2 R \alpha)^{1/2} \tag{2.2}$$

Where: $r$ = Radius of the Indentation
$R$ = Radius of the Indenter
$\alpha$ = Depth of the Indentation

The predominant first occurring failure mode found in composites subjected to low-velocity impact is shear. Using this finding and applying basic strengths of materials relationships the following relation is obtained, Figure 2.4:

$$P = 2 \Pi r h \tau \tag{2.3}$$

Where: $\tau$ = Average Shear Stress
$h$ = Material Thickness

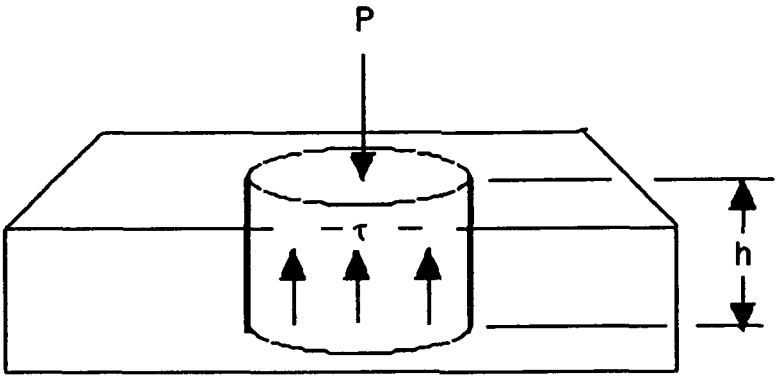


***Figure 2.4. Shear stresses resulting from impact.***

Combining the above equations , the following relation is obtained:

$$P = (2 \Pi h \tau)^{1.5} (2 R)^{0.75} / K_c^{0.5} \qquad (2.4)$$

Where: $K_c$ is proportional to $R^{0.5}$

A third assumption is made that the average shear strength and the elastic properties do not vary with the thickness of the plate. This leads to the final relation which finds the damage initiation force to be a function of material properties, material thickness, and the impacter radius:

$$P_{init} = C\, h^{1.5}\, R^{0.5} \qquad (2.5)$$

Where: $P_{init}$ is the Damage Initiation Force
C is a Material Constant

## 2.3 The Need For a Standardized Low-Velocity Impact Test

Currently there is no standard method for conducting low-velocity impact tests. Each company or institution is conducting low-velocity impact tests on specimens of all different sizes and lay up orientations, supported in a variety of ways, using many different testing techniques. The two most commonly used methods are variations of the method described

in the BSS 7260 document (Boeing) and the method described in the NASA RP 1142 document. Different organizations are currently working on standardization of the Compression-After-Impact (CAI) test where the impact testing is a part of the CAI test.

Low-velocity impact tests do not provide fundamental material properties. Rather, the data obtained from such tests are comparable only to the results of tests run on other materials using the same test method. Since each company is using a different test technique, the comparison of impact data between companies or institutions is virtually impossible. Because of this, a large amount of time and money are wasted by each company testing a particular material using its own low-velocity impact test method. In addition, many of the commonly used methods for conducting low-velocity impact tests have limitations which make them inadequate for evaluating materials. One significant disadvantage is the use of large thick specimens which require a great amount of material. This is often a problem when material is of limited quantity or is very expensive. Another limitation is the fact that many of the low-velocity impact test setups have inadequate instrumentation.

# SECTION 3. EXPERIMENTAL PROCEDURES

## 3.1 Overview

The experimental portion of this investigation consisted of the following: a) Materials, Quality Control and Specimen Preparation; b) Mechanical Testing; and c) Fractographic and Ultrasonic Inspection of Tested Specimens.

## 3.2 Materials Quality Control, and Specimen Preparation

The materials chosen for this investigation include Hercules, AS-4/3502 graphite/epoxy, and ICI's AS-4/APC-2 graphite/PEEK (Polyetheretherketone). These were chosen because they represent materials for which significant data bases exist and because they have very different toughness and ductility characteristics. The AS-4/3502 panels were fabricated and cured in-house according to the manufacturers' recommended cure cycle. The panels consolidated include 8-, 16-, 24-, 34-, and 48-ply laminates. Preconsolidated 8-, 16-, 24-, and 32-ply, AS-4/APC-2 panels were ordered and received from ICI. The quality of the consolidated Hercules, AS-4/3502 and ICI, AS-4/APC-2 panels was checked via ultrasonic inspection of the panels and photomicrographs of representative cross-sections. Once the laminates were determined to be of good quality, various sizes of impact specimens were cut from them using a water-cooled diamond impregnated abrasive saw.

## 3.3 Mechanical Testing

The mechanical testing consisted of both static indentation and low-velocity impact testing. This was done so that the results from the two types of tests could be compared to determine if the assumption of approximately static loading which allows for a static-based analysis was valid.

### 3.3.1 Static Indentation Testing

The static indentation tests were conducted in accordance with the test matrix given in Table 1.1. The tests were conducted using an MTS servohydraulic test machine, shown in Figure 3.1.

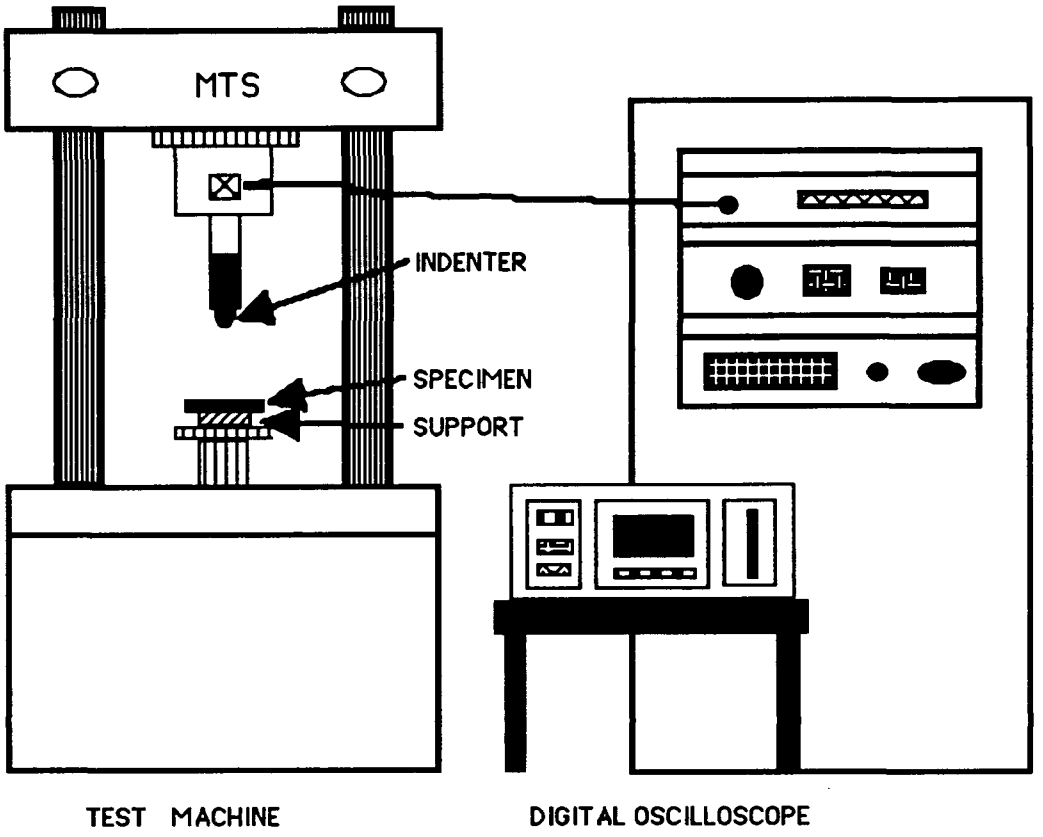


***Figure 3.1. Static indentation experimental setup.***

A 22-kN (5000-lbf) load cell and a ±127-mm (±5-inch) linear variable differential transformer, used in the ±12.7-mm (±0.5-inch) range were used to record the indentation force and depth. A 12.7-mm (0.5-inch) spherical indenter nose was made to fit the existing load cell. Aluminum rings ranging from 25-mm (0.984-in) to 100-mm (3.937-in) diameter were used to support the various sizes of specimens. The specimens were simply laid upon the appropriate size supports, modelling a simply supported test condition. The load and displacement outputs from the MTS system were recorded using a Nicolet 2090 Digital Oscilloscope. A total loading time of approximately one second was used during testing. The data recorded on the oscilloscope were stored on a floppy disk and later transferred to a microcomputer for analysis.

### 3.3.2. Low-Velocity Impact Testing

The low-velocity impact tests were conducted following the test matrix given in Tables 1.1, 1.2 and 1.3. The pendulum type test setup consisted of an impacter suspended from the ceiling by four silicone impregnated Kevlar lines, as seen in Figure 3.2.

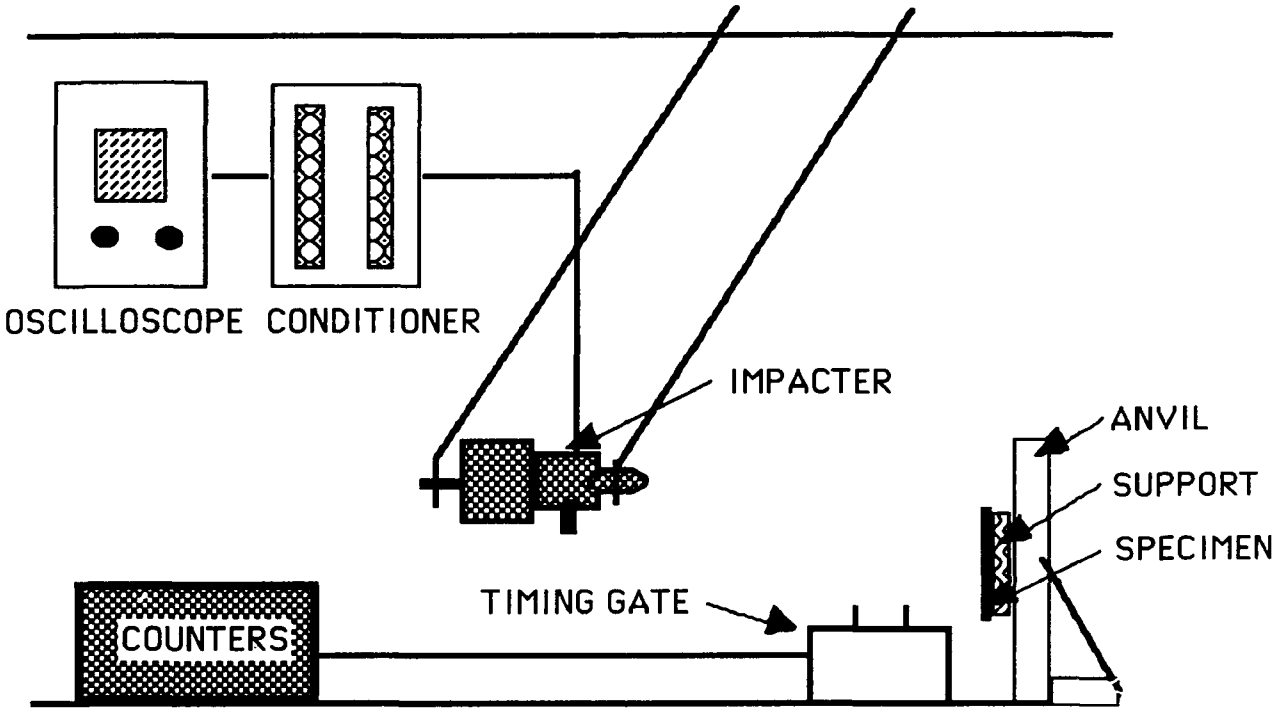


***Figure 3.2. Low-velocity impact test setup.***

The impacter was equipped with a Dynatup 8496-1 load cell, various sizes of removable spherical indenter noses and removable disk weights of varying masses (see Figure 3.3). Connected to the load cell was a Vishay 2310 strain gage conditioner. This setup provided a means of recording force measurements in the 1% accuracy range. A Nicolet 2090 Digital Oscilloscope recorded the voltage (force) versus time data. A timing gate equipped with two pairs of phototransistors and light emitting diodes was connected to two 10-MHz counters. This setup recorded the approach and exit times across the 25.4-mm (1.000 in) gate so that the initial and rebound velocities could be calculated. The accuracy of the data obtained through this setup was in the 0.1% range. A heavy steel anvil, securely bolted to the reinforced concrete laboratory floor, served as a fixture to hold the aluminum specimen

support rings. The appropriate size specimens were affixed to the various size support rings using masking tape. This modelled a simply supported test condition. The Nicolet Oscilloscope was interfaced with an IBM personal computer through an IEEE-488 bus allowing for direct analysis of the recorded data. For Phases 1 and 2, the velocity of the impacter at the time of impact was kept at approximately 1.55 m/s (5.09 ft/s) for each test conducted. This was done by maintaining a pendulum release height of 12.3 cm (4.8 in) throughout the two phases of the investigation. By varying the disk weight the momentum of the impacter was changed to ensure there was a large enough impact force to initiate damage in the plates for the different thicknesses and materials tested.

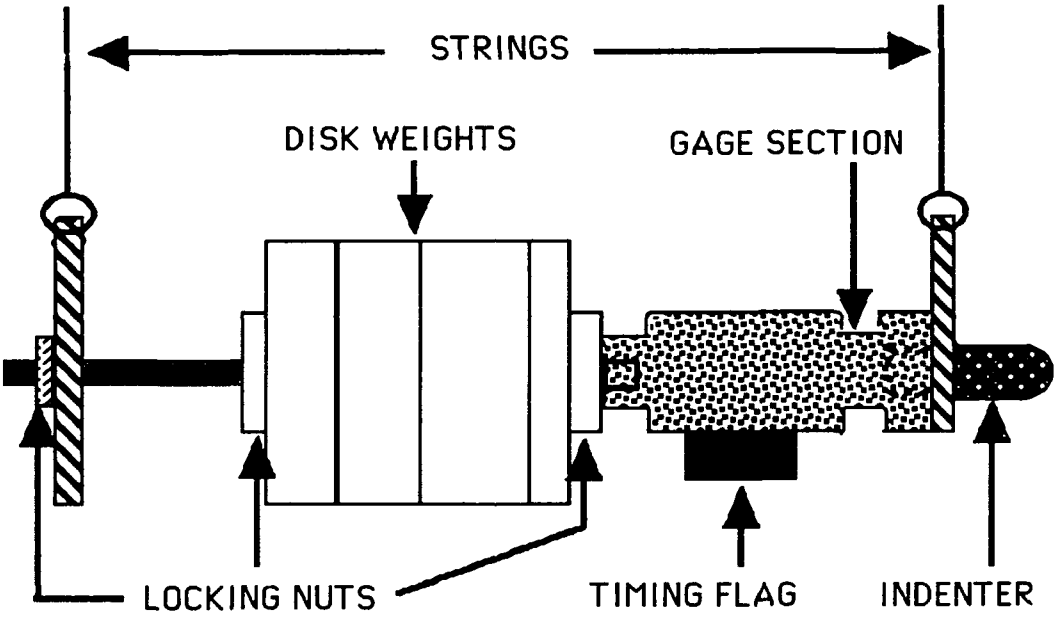


***Figure 3.3. Impacter.***

## 3.4 Fractographic and Ultrasonic Inspection of Tested Specimens

Both the statically indented and impacted specimens were ultrasonically inspected using a conventional C-scan. The specimens were then cross-sectioned through the damaged area using a water cooled diamond edge saw. Photomicrograph plugs were mounted and polished and photomicrographs were taken. The resulting photos were examined for areas showing delaminations, matrix cracking, and fiber breakage.

# SECTION 4. RESULTS

## 4.1 Materials Quality Control

C-Scans and photomicrographs of both the AS-4/3502 and AS-4/APC-2 panels indicated the laminates to be of good quality and to be essentially void free.

## 4.2 Mechanical Testing

### 4.2.1 Static Indentation

The data obtained from the static indentation tests of the graphite/epoxy material are presented in Table 4.1 and plotted in Figure 4.1. It should be noted that initial testing of the 8-ply, graphite/epoxy specimens generated suspicious results. Because analysis of the raw data did not provide any possible explanation for the questionable results, a second set of 8-ply specimens was statically tested. Results from the retests were found to be much more reasonable. Therefore, the data generated from the first set of 8-ply, graphite/epoxy, statically tested specimens were regarded as incorrect. Furthermore, the 75-mm specimen support ring was not available during the retests, and an 80-mm support was used. A non-linear, least squares curve fit was done of the averaged data. The results of this curve fit indicate that for the static case the damage initiation force is proportional to the material thickness raised to approximately the 1.5 power.

***Table 4.1 Averaged Static Graphite/Epoxy Results***

| Thickness (plies) | Supp. Dia. (mm) | Initiation Force (N) |
|---|---|---|
| | | |
| 8 | 25 | 816 |
| 8 | 50 | 744 |
| 8 | 75 | 923 |
| 8 | 100 | 1121 |
| | | |
| 16 | 25 | 1388 |
| 16 | 50 | 1350 |
| 16 | 75 | 1338 |
| 16 | 100 | 1475 |

*continued*

*Table 4.1 Averaged Static Graphite/Epoxy Results (Continued)*

| | | |
|---|---|---|
| 24 | 25 | 2850 |
| 24 | 50 | 2575 |
| 24 | 75 | 2550 |
| 24 | 100 | 2850 |
| | | |
| 32 | 25 | 4950 |
| 32 | 50 | 4600 |
| 32 | 75 | 4600 |
| 32 | 100 | 4450 |

**Phase 1: Graphite/Epoxy Static**

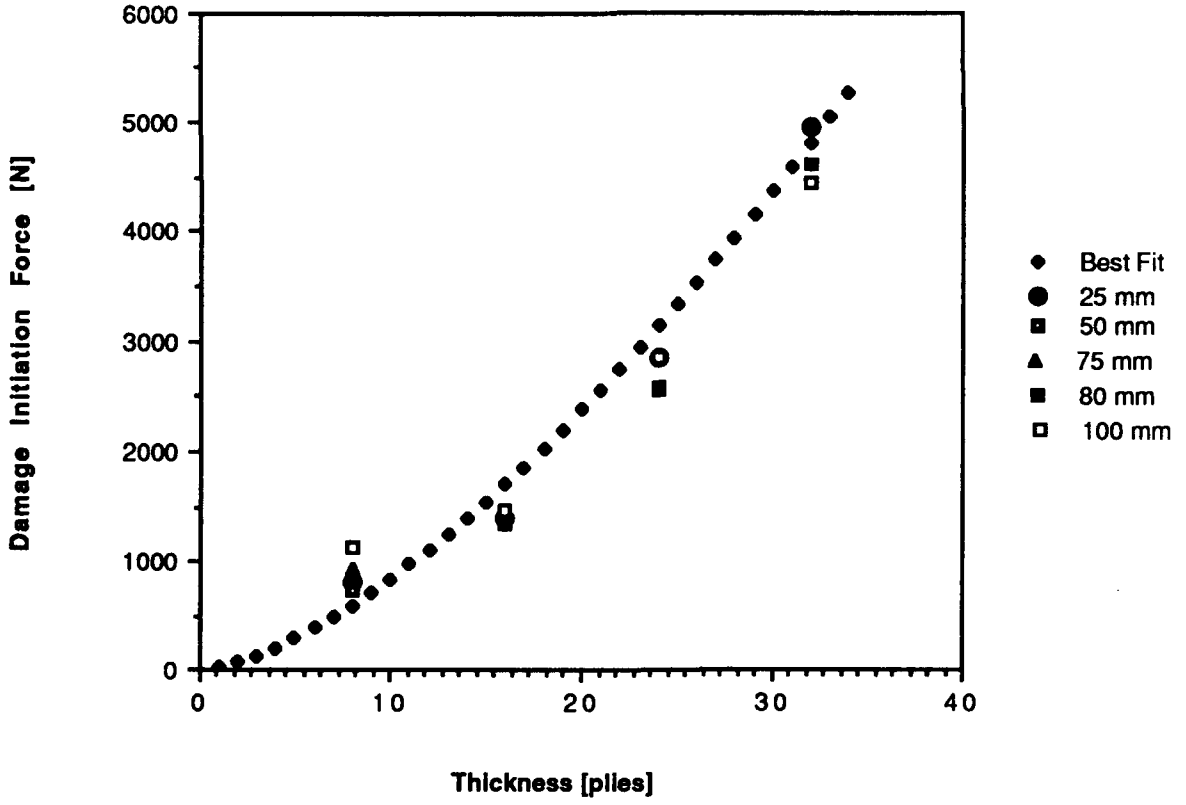


*Figure 4.1. AS-4/3502 static data.*

The results of the static indentation tests conducted on the graphite/PEEK material are given in Table 4.2 and plotted in Figure 4.2. A non-linear, least squares curve fit was done on the averaged data. From the curve fit it appears that the damage initiation force for the thermoplastic matrix material is proportional to the material thickness raised to the 1.5 power. This trend corresponds to the trend predicted by Equation [2.5].

***Table 4.2 Averaged Static Graphite/PEEK Results***

| Thickness (plies) | Supp. Dia. (mm) | Initiation Load (N) |
|---|---|---|
| 8 | 25 | 1015 |
| 8 | 50 | 1138 |
| 8 | 75 | 1345 |
| 8 | 100 | 1015 |
| 16 | 25 | 3143 |
| 16 | 50 | 2585 |
| 16 | 75 | 2653 |
| 16 | 100 | 2848 |
| 24 | 25 | 6200 |
| 24 | 50 | 5450 |
| 24 | 75 | 5000 |
| 24 | 100 | 5000 |
| 32 | 25 | 9785 |
| 32 | 50 | 8740 |
| 32 | 75 | 7795 |
| 32 | 100 | 7538 |

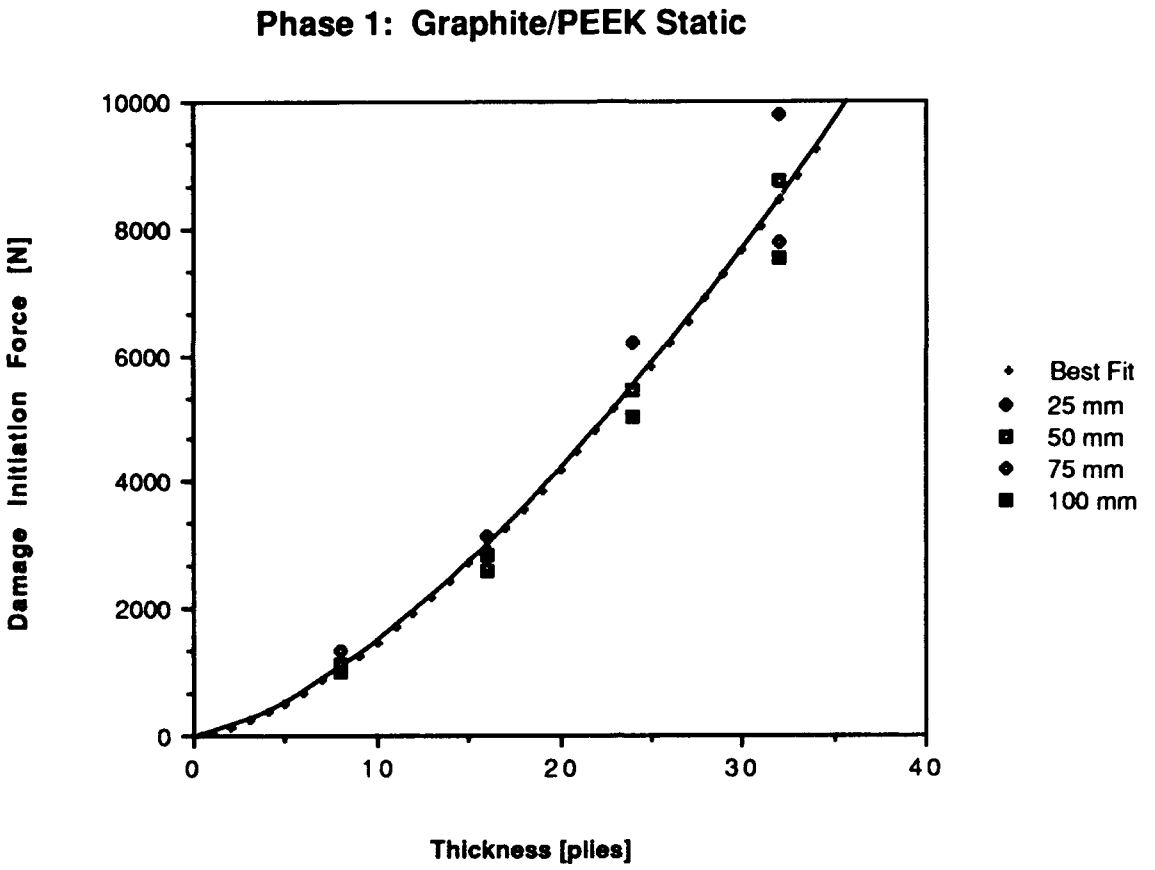


***Figure 4.2. AS-4/APC-2 static data.***

### 4.2.2 Low Velocity Impact

The averaged graphite/epoxy data obtained for Phase 1 of this investigation is given in Table 4.3. The numbers in parentheses are the standard deviations for the given set of averaged data. These data are also plotted in Figures 4.3 and 4.4. A non-linear, least squares curve fit was performed on the damage initiation force versus thickness data in Figure 4.3. This was done so that the resulting trend might be compared to the trend predicted by the aforementioned mathematical relationship. From the plot in Figure 4.3 it can be noted that the damage initiation force appears to be a function of the material thickness raised to the 1.5 power. This result correlates well with the trend predicted by the mathematical model. The plot in Figure 4.4 indicates that the damage initiation force is essentially independent of specimen support diameter.

***Table 4.3 Phase 1: Averaged Graphite/Epoxy Results***

| Thick. (plies) | Supp. Dia (mm) | Damage Initiation Force (N) | Energy (J) | Impact Velocity (m/s) | Energy Loss (%) |
|---|---|---|---|---|---|
| 8 | 25 | 1136 (46) | 0.730(.054) | 1.558(.019) | 90.7(0.8) |
| 8 | 50 | 1013(88) | 0.905(.088) | 1.567(.008) | 85.8(2.0) |
| 8 | 75 | 1052(137) | 1.182(.182) | 1.628(.152) | 75.2(3.1) |
| 8 | 100 | 1031(45) | 1.395(.059) | 1.560(.015) | 70.0(2.5) |
| 16 | 25 | 1633(24) | 0.450(.063) | 1.565(.025) | 63.3(7.3) |
| 16 | 50 | 1494(65) | 0.863(.034) | 1.556(.007) | 48.3(7.9) |
| 16 | 75 | 1519(53) | 1.310(.077) | 1.571(.007) | 64.6(3.0) |
| 16 | 100 | 1566(54) | 1.824(.118) | 1.578(.0130 | 74.4(2.1) |
| 24 | 25 | 3431(53) | 0.803(.039) | 1.525(.007) | 62.3(0.4) |
| 24 | 50 | 2905(52) | 1.465(.192) | 1.562(.007) | 53.6(1.2) |
| 24 | 75 | 2959(171) | 2.400(.104) | 1.585(.004) | 38.6(1.1) |
| 24 | 100 | 3217(103) | 3.750(.168) | 1.599(.007) | 60.2(5.3) |
| 32 | 25 | 5079(310) | 1.500(.107) | 1.587(.008) | 59.7(0.3) |
| 32 | 50 | 5233(151) | 2.291(.135) | 1.590(.004) | 57.8(0.7) |
| 32 | 75 | 5061(56) | 3.576(.352) | 1.589(.005) | 51.4(2.5) |
| 32 | 100 | 4655(76) | 4.787(.309) | 1.597(.003) | 38.1(1.8) |
| 48 | 25 | 10350(352) | 4.325(.214) | 1.596(.009) | 61.6(0.4) |
| 48 | 50 | 9911(58) | 4.749(.175) | 1.610(.006) | 60.7(0.5) |
| 48 | 75 | 9629(368) | 6.179(.407) | 1.608(.010) | 57.3(1.5) |
| 48 | 100 | 9621(285) | 8.058(.299) | 1.615(.010) | 53.9(1.1) |

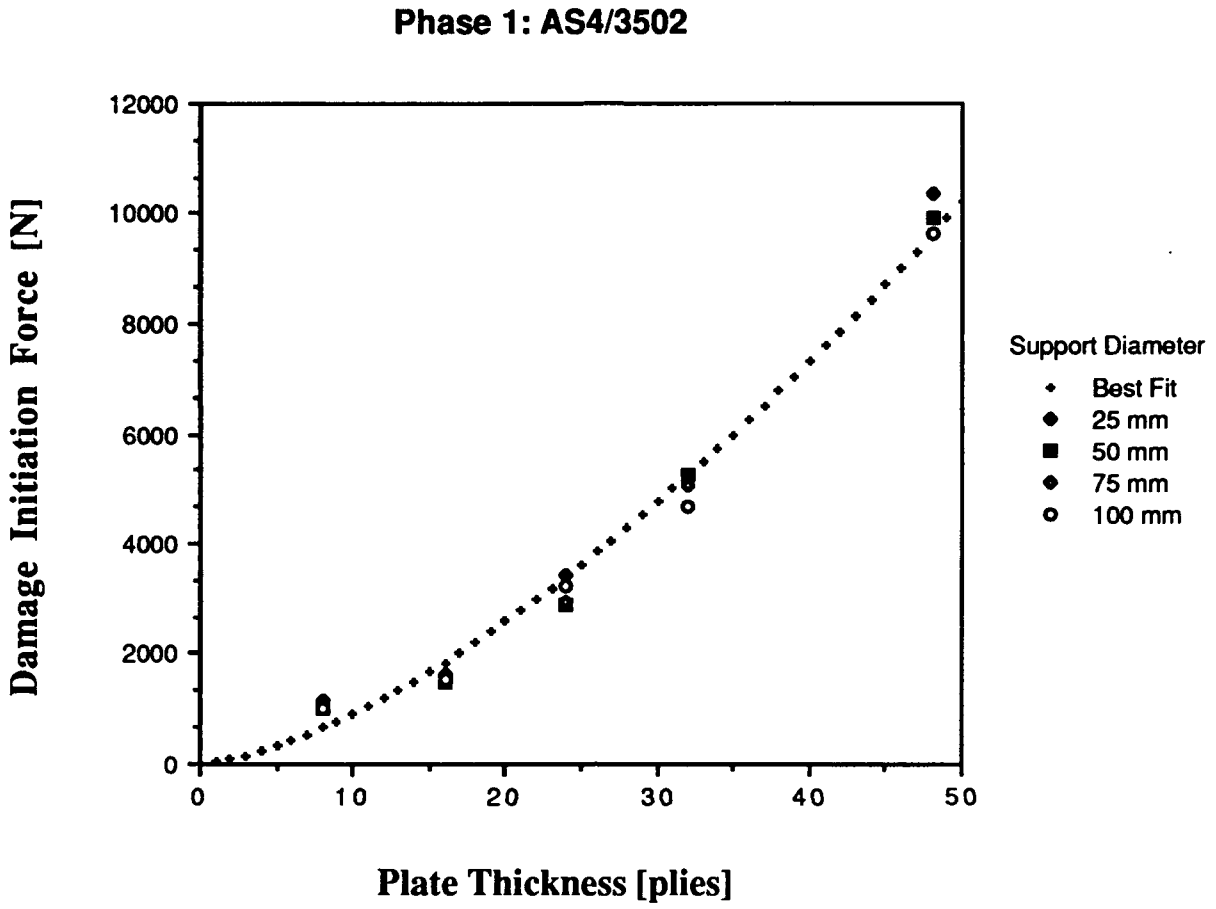


*Figure 4.3. Phase 1: AS-4/3502 data.*

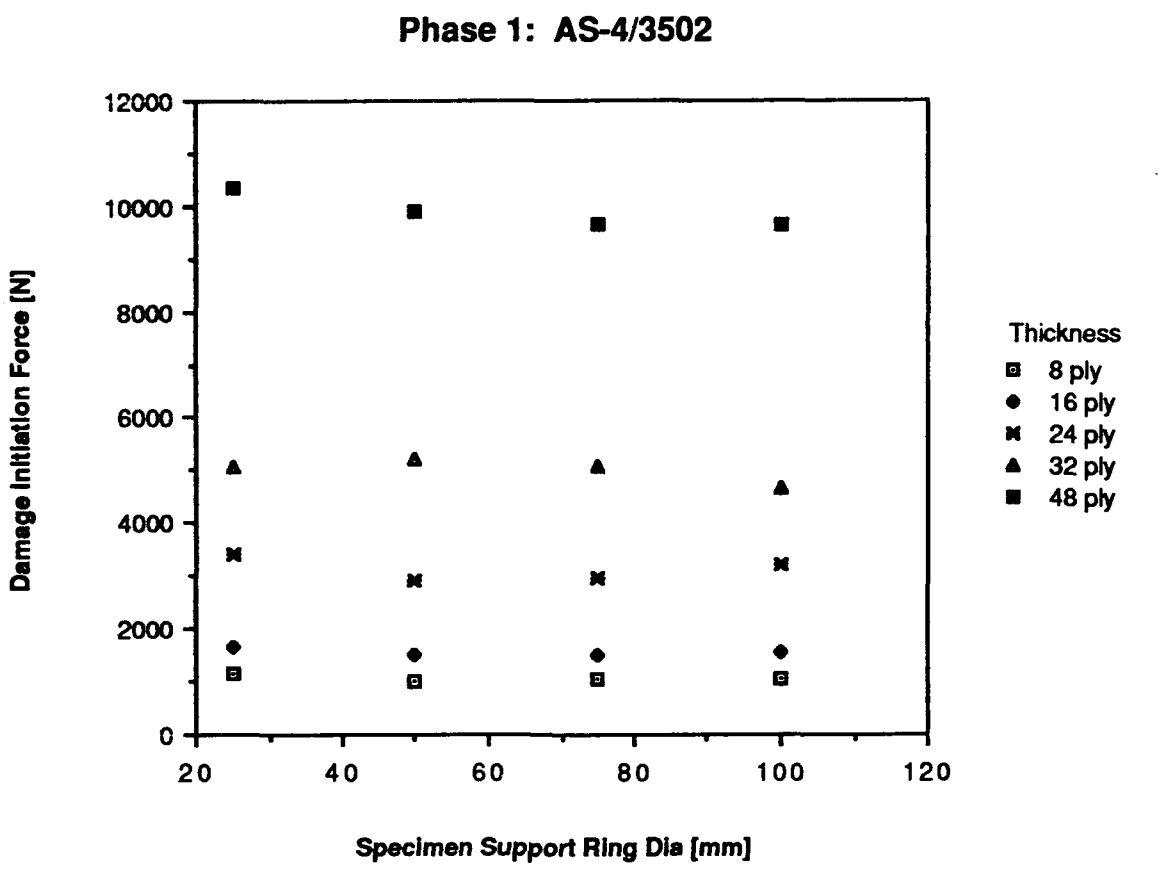


***Figure 4.4. Phase 1: AS-4/3502 data.***

The average data generated in Phase 1 for the graphite/PEEK material is presented in Table 4.4 and plotted in Figures 4.5 and 4.6 As with the graphite/epoxy material a non-linear, least squares curve fit was performed on the damage initiation force versus specimen thickness data in Figure 4.5. Examination of Figure 4.5 indicates that the damage initiation force is a function of the material thickness raised to the 1.5 power. This result also correlates well with the trend predicted by the mathematical model. The plot in Figure 4.6 indicates that the damage initiation force is essentially independent of specimen support size.

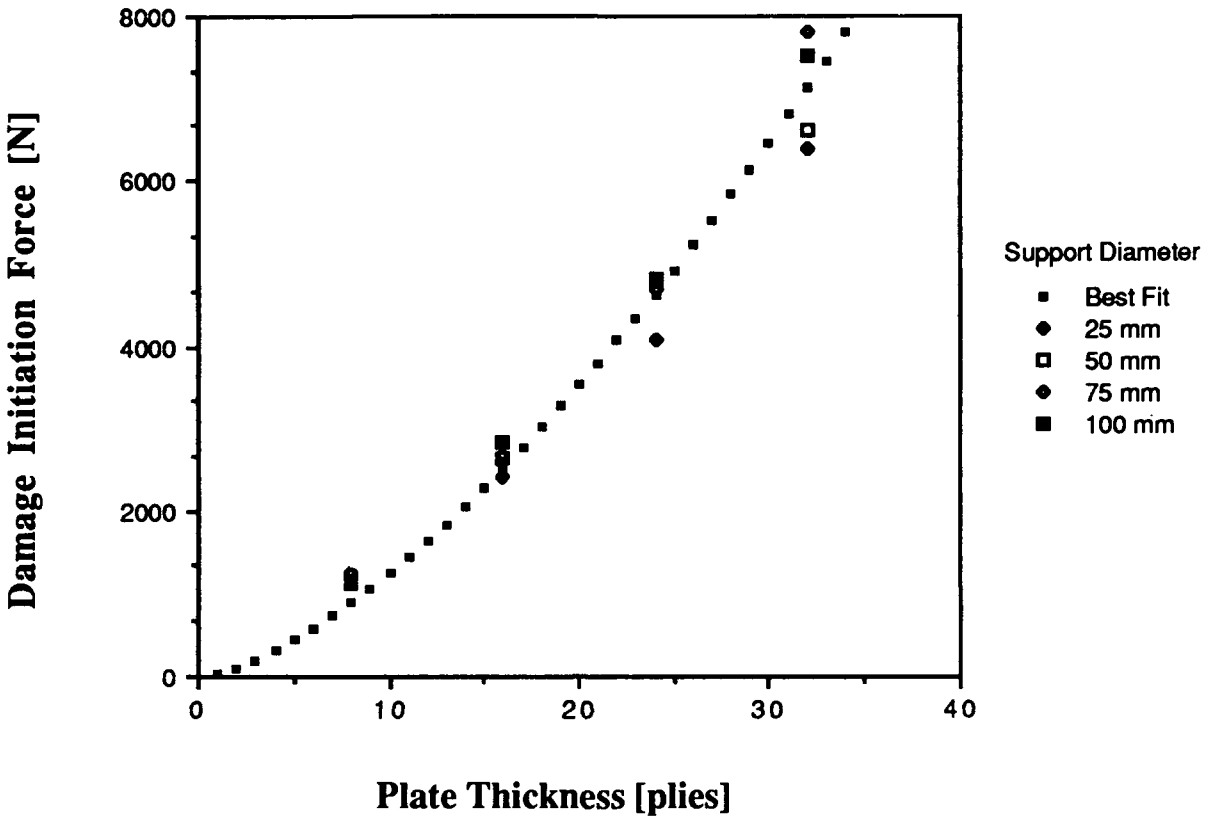


***Figure 4.5. Phase 1: AS-4/APC-2 data.***

***Table 4.4 Phase 1: Averaged Graphite/PEEK Results.***

| Thick. (plies) | Supp. Dia (mm) | Damage Initiation Force (N) | Damage Initiation Energy (J) | Impact Velocity (m/s) | Energy Loss (%) |
|---|---|---|---|---|---|
| | | | | | |
| 8 | 25 | 1176(67) | .615(.054) | 1.622(.024) | 84.0(1.3) |
| 8 | 50 | 1118(52) | .960(.049) | 1.600(.014) | 72.4(1.2) |
| 8 | 75 | 1240(24) | 1.368(.068) | 1.547(.020) | 57.5(1.1) |
| 8 | 100 | 1168(144) | 1.624(.251) | 1.560(.011) | 46.8(6.4) |
| | | | | | |
| 16 | 25 | 2423(218) | 1.144(.148) | 1.548(.006) | 59.6(2.1) |
| 16 | 50 | 2626(171) | 2.262(.241) | 1.556(.011) | 42.4(3.4) |
| 16 | 75 | 2658(96) | 3.341(.155) | 1.563(.009) | 45.7(2.2) |
| 16 | 100 | 2835(101) | 4.390(.154) | 1.577(.020) | 51.3(3.9) |

*Continued*

*Table 4.4 Phase 1: Averaged Graphite/PEEK Results (Continued).*

| | | | | | |
|---|---|---|---|---|---|
| 24 | 50 | 4758(385) | 3.913(.392) | 1.576(.007) | 61.0(4.0) |
| 24 | 75 | 4690(279) | 4.873(.078) | 1.568(.016) | 39.8(1.4) |
| 24 | 100 | 4808(132) | 6.884(.069) | 1.577(.007) | 31.7(1.2) |
| | | | | | |
| 32 | 25 | 6401(320) | 2.670(.284) | 1.586(.011) | 61.9(1.7) |
| 32 | 50 | 6616(322) | 4.385(.260) | 1.564(.003) | 58.2(3.9) |
| 32 | 75 | 7796(174) | 9.125(.447) | 1.575(.009) | 48.9(2.4) |
| 32 | 100 | 7524(413) | 11.428(1.323) | 1.869(.171) | 43.6(12.6) |

**Phase 1: AS-4/APC-2**

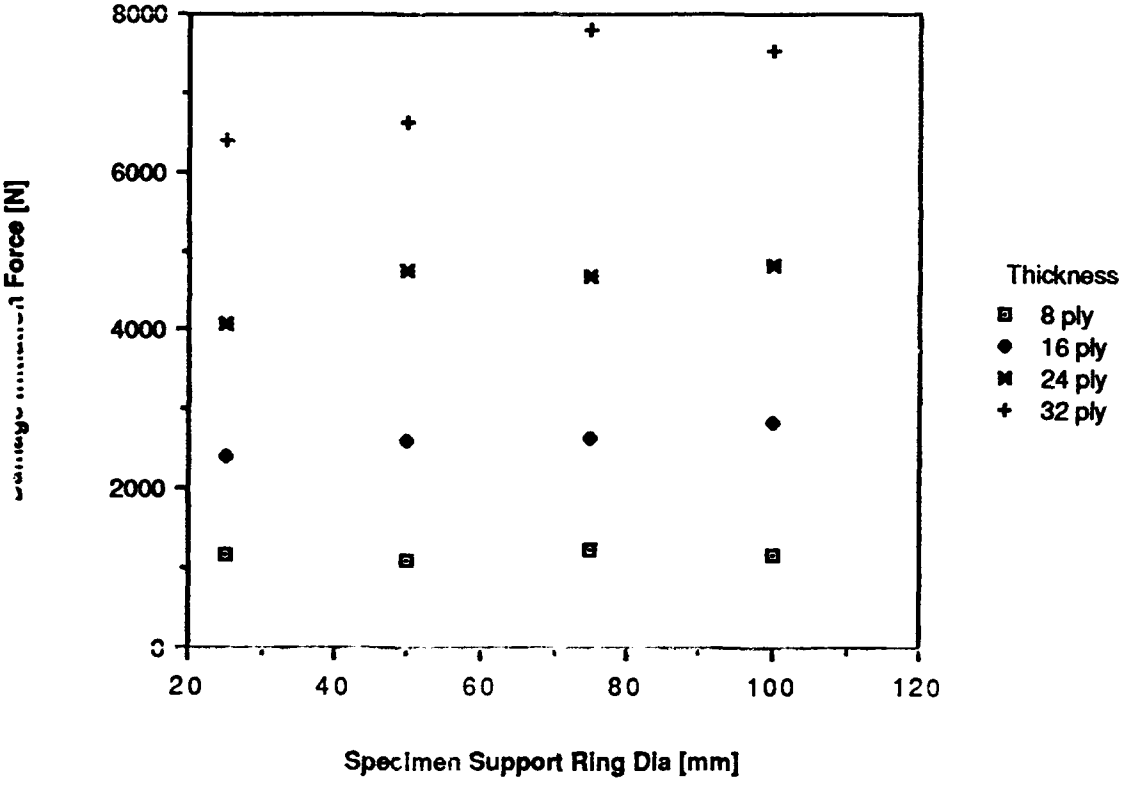


*Figure 4.6. Phase 1: AS-4/APC-2 data.*

The averaged Phase 2 data obtained for the graphite/epoxy material are shown in Table 4.5 and plotted in Figure 4.7. A non-linear curve fit of the data indicates that the damage initiation force is a function of the indenter nose diameter raised to the 0.25 power. This trend is slightly different from that predicted by the mathematical model, equation 2.5. Furthermore, since the curves in Figure 4.7 are not superimposed for a given material thickness, the damage initiation force does not appear to be independent of specimen support size. This contradicts what was found in Phase 1 of this investigation.

***Table 4.5 Phase 2: Averaged Graphite/Epoxy Results***

| 25 mm Dia Support: | | | | | |
|---|---|---|---|---|---|
| | Nose | Damage | Initiation | Impact | Energy |
| Thick. | Dia | Force | Energy | Velocity | Loss |
| (plies) | (mm) | (N) | (J) | (m/s) | (%) |
| | | | | | |
| 32 | 6.35 | 5460(161) | 1.998(.221) | 1.602(.004) | 66.8(1.1) |
| 32 | 12.7 | 6206(165) | 1.995(.045) | 1.600(.004) | 62.9(1.2) |
| 32 | 25.4 | 7410(430) | 2.265(.208) | 1.596(.006) | 61.8(1.3) |
| | | | | | |
| 50 mm Dia Support: | | | | | |
| | Nose | Damage | Initiation | Impact | Energy |
| Thick. | Dia | Force | Energy | Velocity | Loss |
| (plies) | (mm) | N) | (J) | (m/s) | (%) |
| | | | | | |
| 16 | 6.35 | 1375(25) | 0.660(.021) | 1.613(.003) | 86.2(2.7) |
| 16 | 12.7 | 1668(8) | 0.855(.086) | 1.598(.003) | 71.0(1.6) |
| 16 | 25.4 | 2000(28) | 1.073(.044) | 1.612(.008) | 44.2(1.6) |
| 16 | 50.8 | 1900(274) | N/A | 1.608(.009) | 37.2(0.7) |
| | | | | | |
| 32 | 6.35 | 4995(79) | 2.070(.106) | 1.613(.006) | 58.2(0.3) |
| 32 | 12.7 | 5945(231) | 2.423(.206) | 1.592(.008) | 59.2(1.0) |
| 32 | 25.4 | 7173(217) | 3.170(.121) | 1.612(.004) | 59.3(0.3) |
| 32 | 50.8 | 8665(398) | 4.770(.114) | 1.612(.005) | 61.6(0.5) |

*Continued*

*Table 4.5 Phase 2: Averaged Graphite/Epoxy Results (Continued)*

| 100 mm Dia Support: | | | | | |
|---|---|---|---|---|---|
| | Nose | Damage | Initiation | Impact | Energy |
| Thick. | Dia | Force | Energy | Velocity | Loss |
| (plies) | (mm) | (N) | (J) | (m/s) | (%) |
| | | | | | |
| 16 | 6.35 | 1510(39) | 1.560(.139) | 1.596(.005) | 63.1(1.0) |
| 16 | 12.7 | 1578(53) | 1.848(.122) | 1.587(.013) | 74.4(2.1) |
| 16 | 25.4 | 1827(77) | 2.000(.079) | 1.608(.007) | 21.1(0.4) |
| 16 | 50.8 | 2320(14) | 2.742(.135) | 1.608(.006) | 30.4(8.2) |
| | | | | | |
| 32 | 6.35 | 4780(314) | 3.680(.184) | 1.566(.022) | 45.3(2.0) |
| 32 | 12.7 | 4676(121) | 5.028(.336) | 1.598(.003) | 38.3(1.7) |
| 32 | 25.4 | 6190(222) | 5.766(.360) | 1.614(.005) | 56.9(3.5) |
| 32 | 50.8 | 7040(466) | 6.525(.168) | 1.612(.006) | 46.2(1.7) |

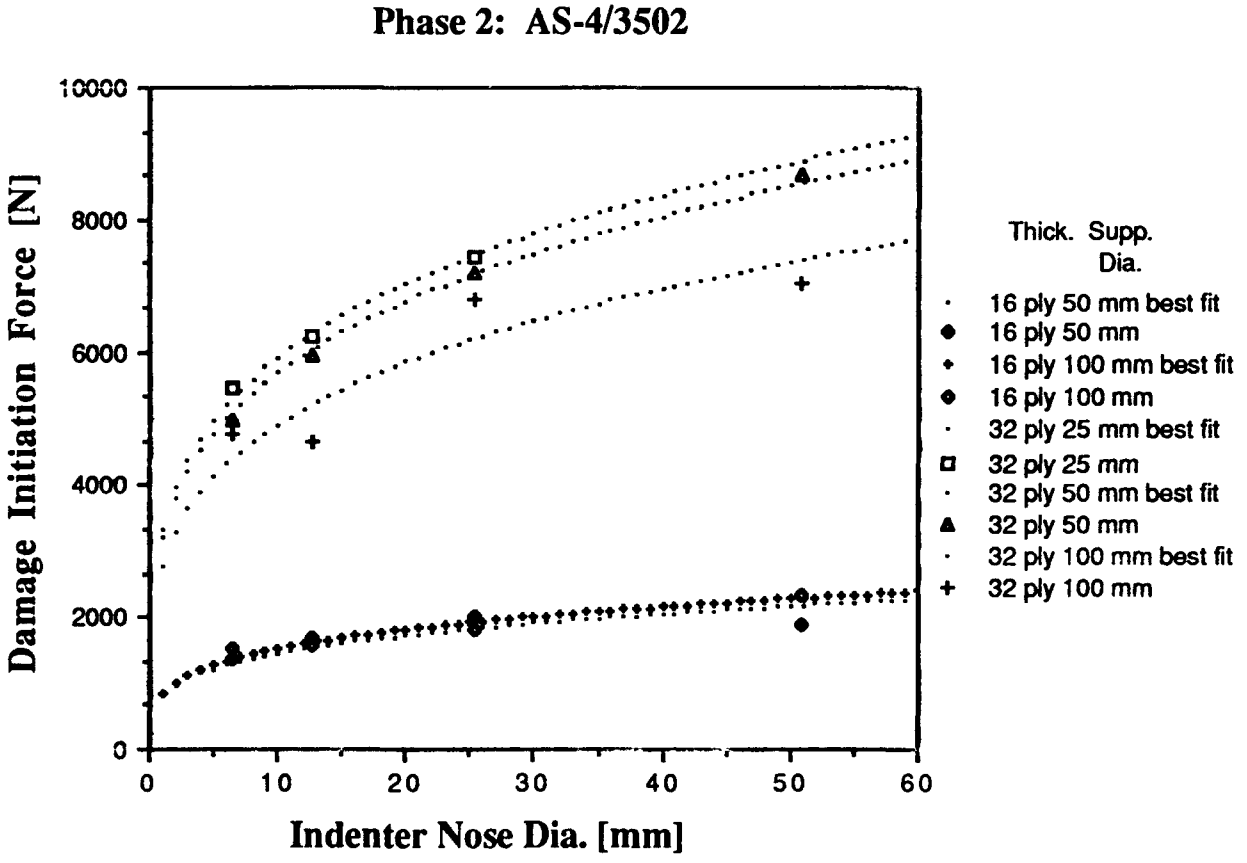


*Figure 4.7. Phase 2: AS-4/3502 data.*

The averaged Phase 2 data obtained for the graphite/PEEK material is presented in Table 4.6 and plotted in Figure 4.8. From Figure 4.8 it appears that for the graphite/PEEK material the damage initiation force is a function of the indenter nose diameter raised to the 0.25 power. This is identical to the trend found for the graphite/epoxy material. As with the graphite/epoxy material, the damage initiation force for the graphite/PEEK material does not appear to be independent of specimen support size.

***Table 4.6 Phase 2: Averaged Graphite/PEEK Results.***

| 50 mm Dia Support | | | | | |
|---|---|---|---|---|---|
| | Nose | Damage Initiation | | Impact | Energy |
| Thick. | Dia. | Force | Energy | Velocity | Loss |
| (plies) | (mm) | (N) | (J) | (m/s) | (%) |
| | | | | | |
| 16 | 6.35 | 4200(200) | N/A | 1.572(.000) | 100.0(0.0) |
| 16 | 12.7 | 2653(52) | 2.120(.196) | 1.574(.011) | 52.7(1.3) |
| 16 | 25.4 | 3266(125) | 2.900(.071) | 1.577(.006) | 36.2(2.9) |
| 16 | 50.8 | 4500(75) | 4.450(.283) | 1.580(.005) | 28.0(3.2) |
| | | | | | |
| 32 | 6.35 | 6300(245) | 4.220(.449) | 1.578(.007) | 49.6(1.2) |
| 32 | 12.7 | 6520(227) | 3.770(.422) | 1.591(.005) | 8.5(3.4) |
| 32 | 25.4 | 8400(283) | 5.750(1.251) | 1.586(.006) | 33.4(1.8) |
| 32 | 50.8 | 12020(534) | 11.333(1.236) | 1.584(.004) | 37.4(0.6) |
| | | | | | |
| 100 mm Dia Support | | | | | |
| | Nose | Damage Initiation | | Impact | Energy |
| Thick. | Dia. | Force | Energy | Velocity | Loss |
| (plies) | (mm) | (N) | (J) | (m/s) | (%) |
| | | | | | |
| 16 | 6.35 | 4100(1283) | 3.450(N/A) | 1.577(.005) | 88.2(16.7) |
| 16 | 12.7 | 2600(51) | 4.160(.681) | 1.578(.005) | 38.9(16.7) |
| 16 | 25.4 | 3413(19) | 5.350(.187) | 1.583(.001) | 24.2(0.9) |
| 16 | 50.8 | 3880(267) | 5.410(.781) | 1.577(.007) | 16.8(0.6) |
| | | | | | |
| 32 | 6.35 | 6093(82) | 8.950(.430) | 1.578(.010) | 22.9(2.3) |
| 32 | 12.7 | 6767(287) | 10.000(.748) | 1.592(.001) | 21.7(1.7) |
| 32 | 25.4 | 7780(380) | 12.200(.600) | 1.585(.003) | 17.1(5.2) |
| 32 | 50.8 | 9000(N/A) | 15.600(N/A) | 1.674(.062) | 9.9(1.7) |
| | | | | | |

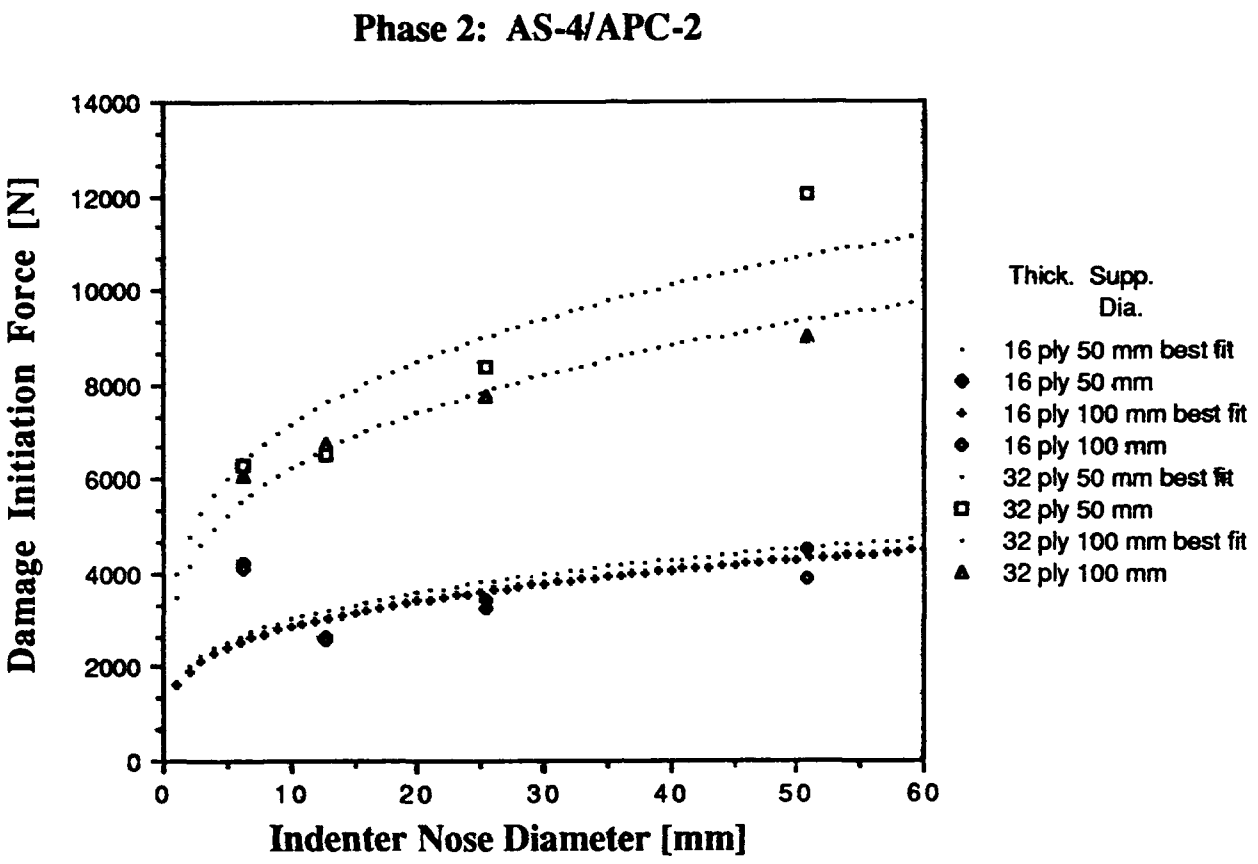


***Figure 4.8. Phase 2: AS-4/APC-2 data.***

Phase 2 data indicate that the damage initiation force is not independent of the specimen support size. This contradicts what was found in Phase 1 of this investigation. In attempts to determine why the Phase 2 data do not correspond to the Phase 1 data, a statistical analysis was done on the experimental data. An Analysis of Variance table and variable interaction plots were generated, as shown in Tables 4.7 and 4.8 and in Figures 4.9 through 4.12. The resulting information indicates that it is likely that there is an interaction effect between the indenter nose diameter, specimen support size, and material thickness for both materials. Therefore, it is likely that the damage initiation force is independent of the specimen support size for a given indenter nose diameter.

***Table 4.7 Phase 2: Graphite/Epoxy Analysis of Variance***

| SOURCE | DOF | SS | MS | F | P |
|---|---|---|---|---|---|
| A | 1 | 310667072 | 310667072 | 5193.14 | 0.000 |
| B | 1 | 3603353 | 3603353 | 60.23 | 0.000 |
| C | 3 | 32482718 | 10827573 | 180.99 | 0.000 |
| A*B | 1 | 4884100 | 4884100 | 81.64 | 0.000 |
| A*C | 3 | 13530694 | 4510231 | 75.39 | 0.000 |
| B*C | 3 | 1028589 | 342863 | 5.73 | 0.002 |
| A*B*C | 3 | 1552750 | 517583 | 8.65 | 0.000 |
| ERROR | 48 | 2871484 | 59823 | | |
| TOTAL | 63 | 370620736 | | | |

Where: A = Thickness
B = Specimen Support Size
C = Indenter Nose Diameter

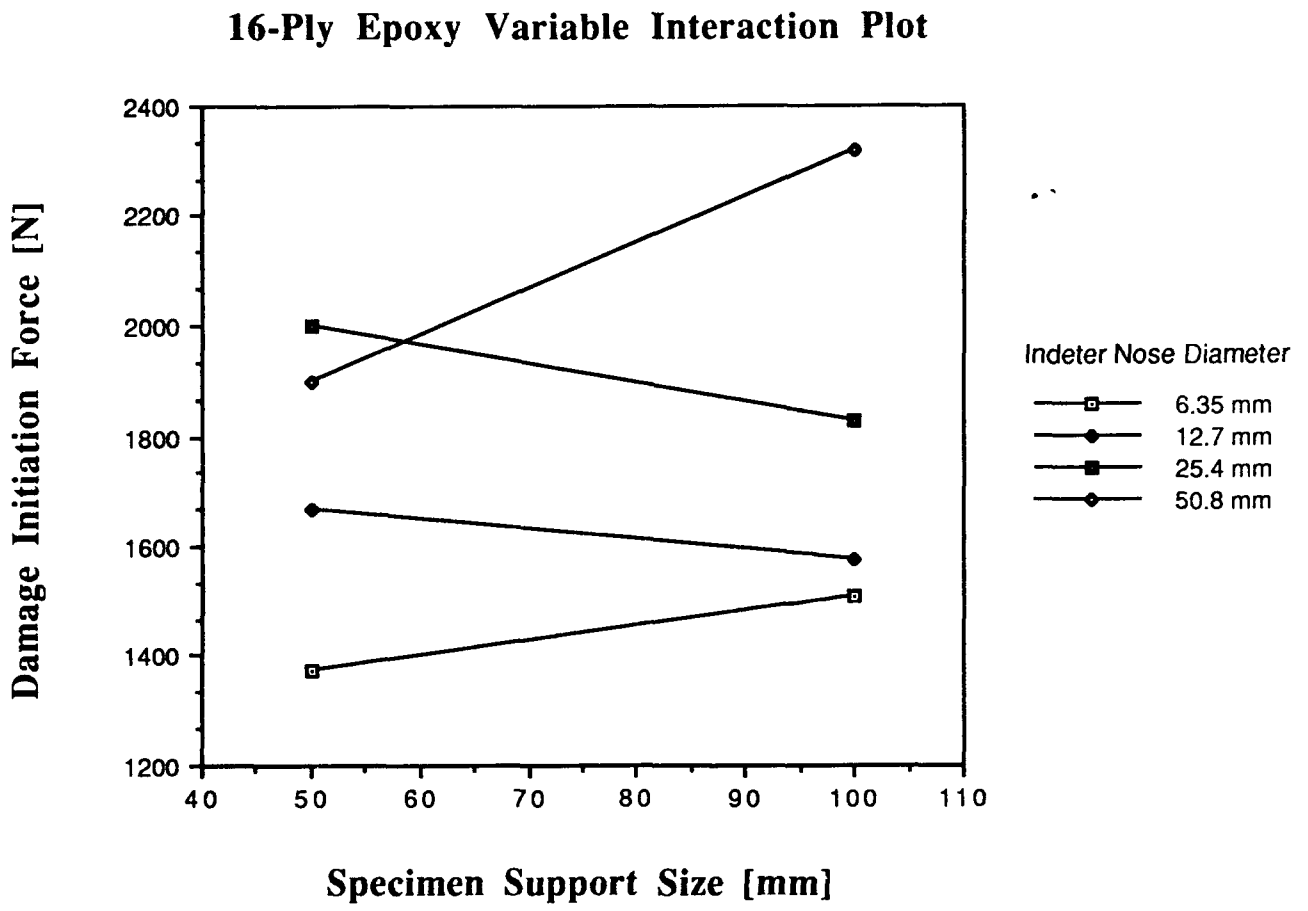


*Figure 4.9. 16-Ply AS-4/3502 variable interaction plot.*

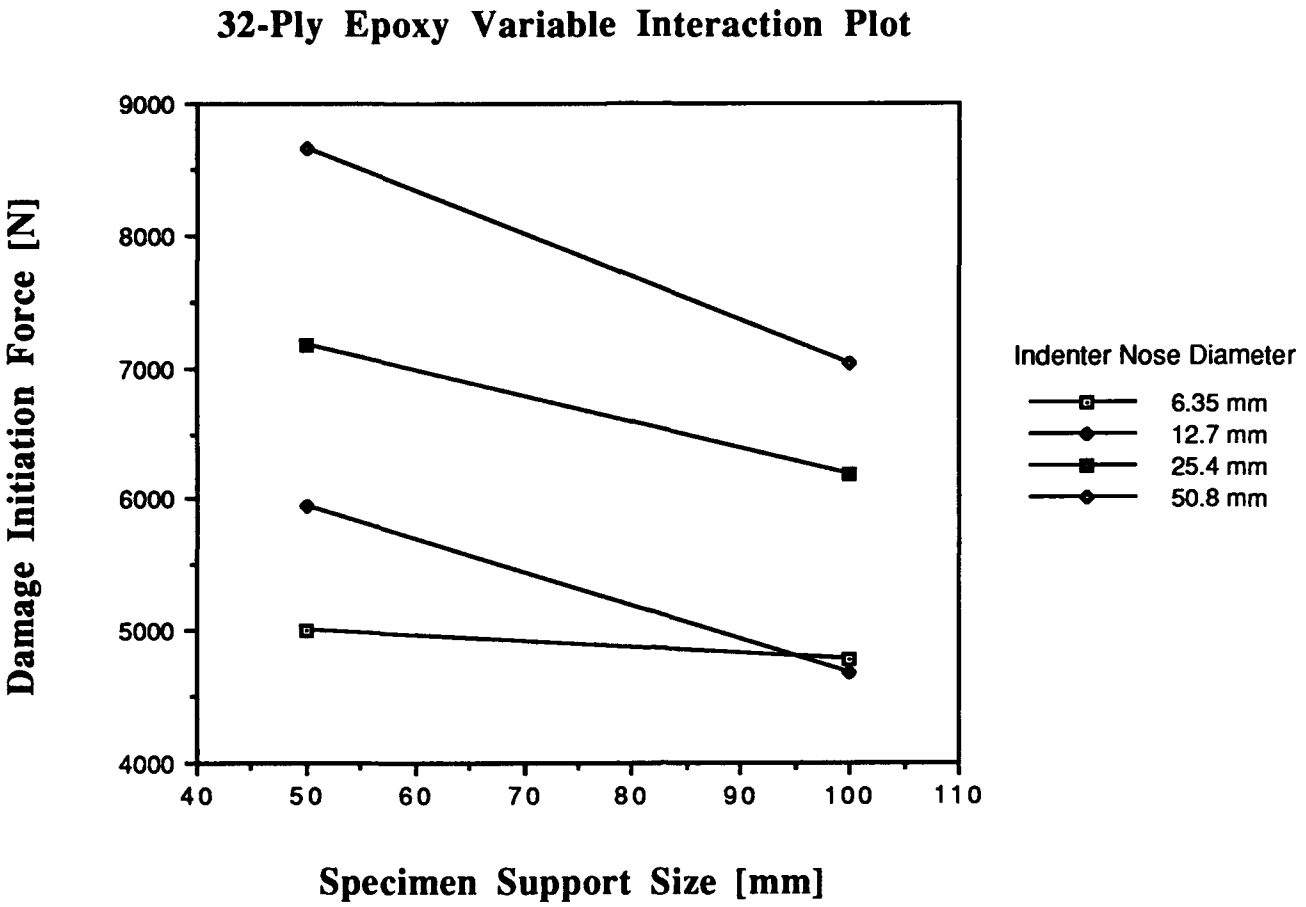


*Figure 4.10. 32-Ply AS-4/3502 variable interaction plot.*

*Table 4.8 Phase 2: Graphite/PEEK Analysis of Variance*

| SOURCE | DOF | SS | MS | F | P |
|---|---|---|---|---|---|
| A | 1 | 260028304 | 260028304 | 1120.99 | 0.000 |
| B | 1 | 294533 | 294533 | 1.27 | 0.268 |
| C | 3 | 63357232 | 21119077 | 91.05 | 0.000 |
| A*B | 1 | 5880000 | 5880000 | 25.35 | 0.000 |
| A*C | 3 | 14018300 | 4672767 | 20.14 | 0.000 |
| B*C | 3 | 14400733 | 4800244 | 20.69 | 0.000 |
| A*B*C | 3 | 510867 | 170289 | 7.34 | 0.001 |
| ERROR | 32 | 7422800 | 231963 | | |
| TOTAL | 47 | 370509952 | | | |

Where: A = Thickness
B = Specimen Support Size
C = Indenter Nose Diameter

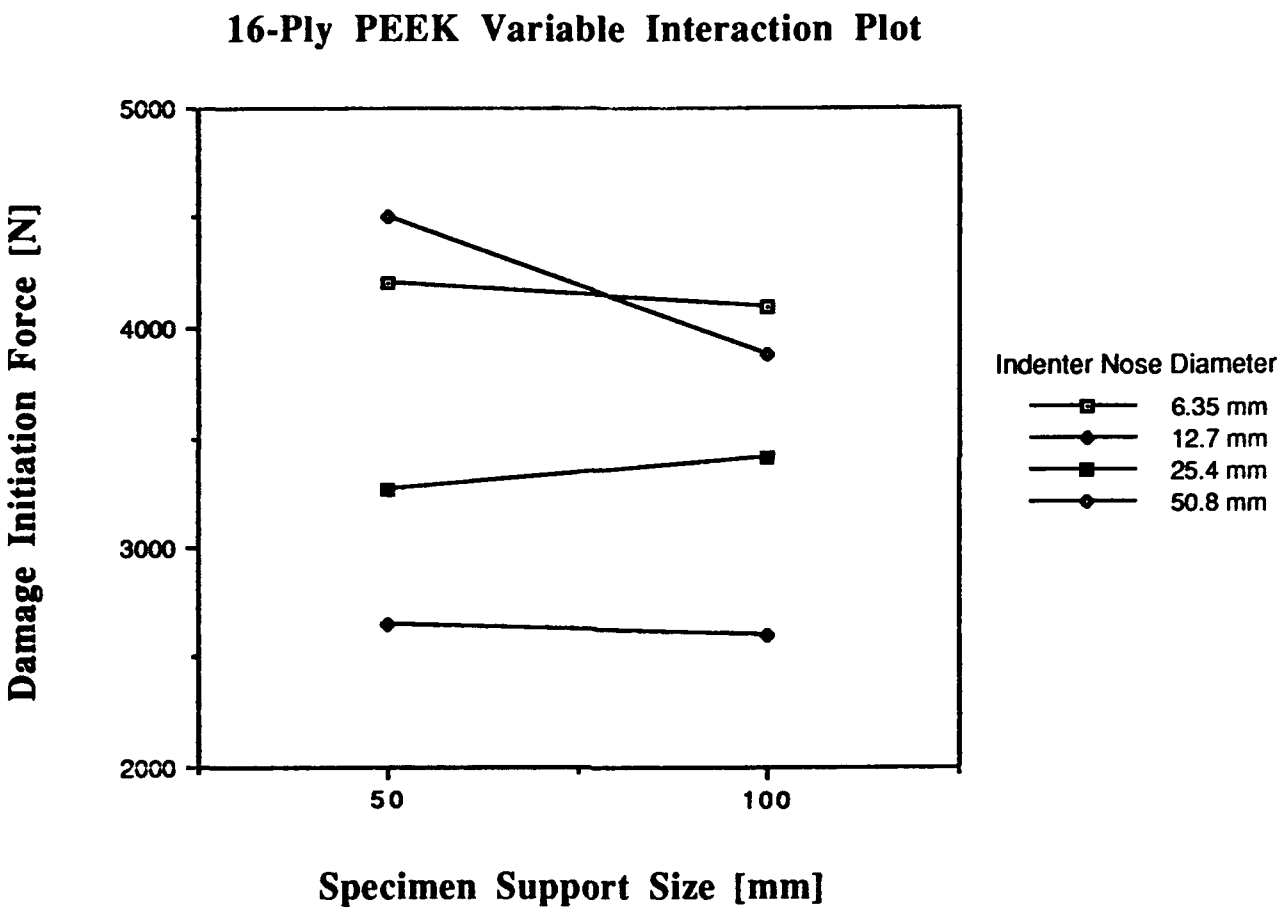


*Figure 4.11. 16-Ply AS-4/APC-2 variable interaction plot.*

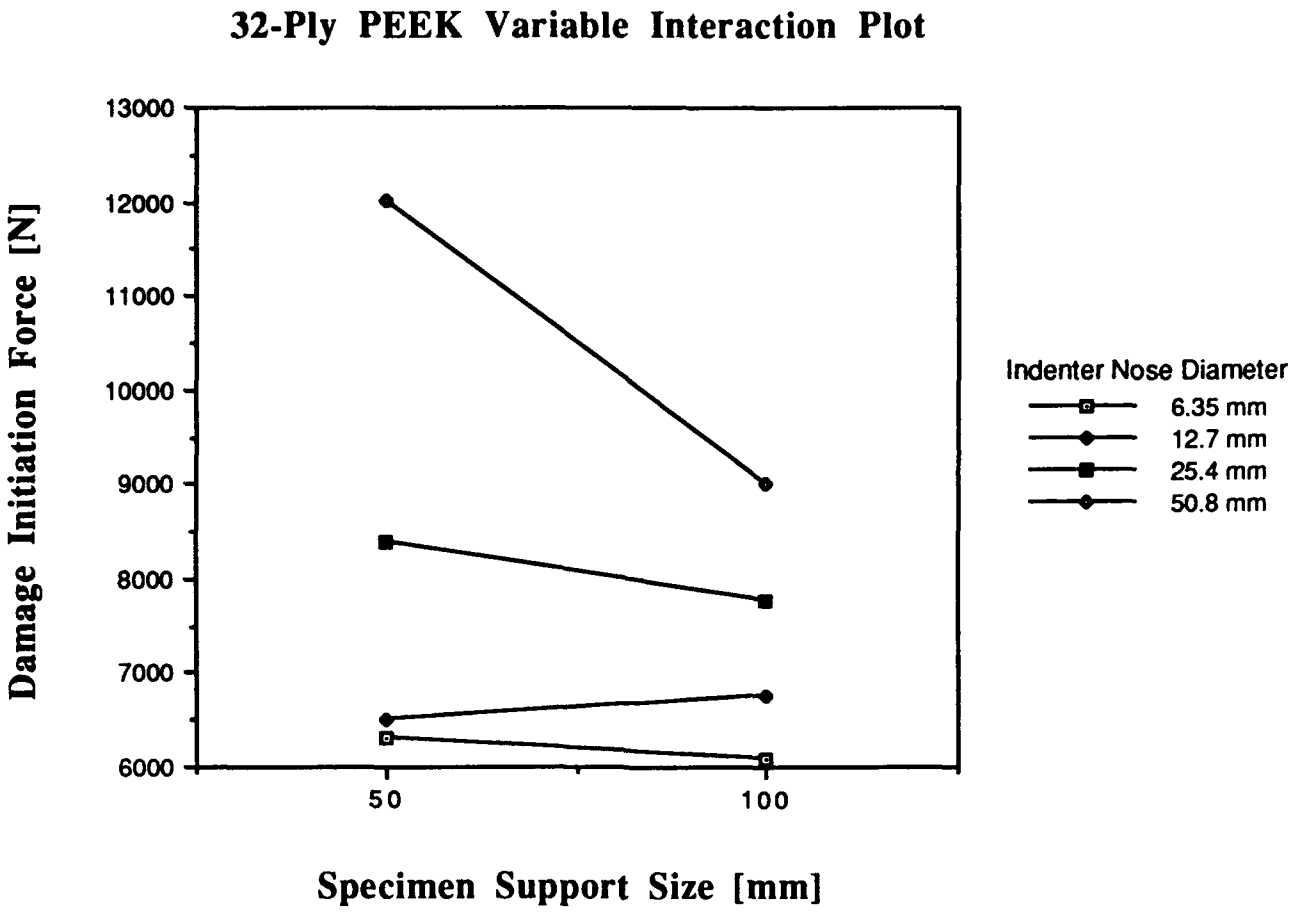


***Figure 4.12. 32-Ply AS-4/APC-2 variable interaction plot.***

The averaged Phase 3 data for the graphite/epoxy material are presented in Table 4.9 and are plotted in Figure 4.13. Inspection of the plot in Figure 4.13 indicates that for this material the damage initiation force is essentially independent of impact velocity for the range of velocities tested.

***Table 4.9 Phase 3: Averaged Graphite/Epoxy Results***

| 50 mm Dia. Support | | | | | |
|---|---|---|---|---|---|
| | Vel. | Damage Initiation | | Impact | Energy |
| Thick. | Code | Load | Energy | Velocity | Loss |
| (plies) | | (N) | (J) | (m/s) | (%) |
| | | | | | |
| 16 | A | 2100(500) | 0.700(.000) | 1.332(.003) | 83.9(1.3) |
| 16 | B | 1713(152) | 1.450(.456) | 2.003(.003) | 83.5(1.0) |
| 16 | C | 1913(228) | 0.900(.300) | 2.958(.021) | 53.0(2.7) |
| 16 | D | 1936(54) | 0.867(.189) | 3.908(.016) | 56.9(2.9) |
| 16 | E | 2165(145) | 1.225(.349) | 4.762(.015) | 47.1(5.5) |
| | | | | | |
| 32 | A | 6235(181) | 2.575(.130) | 1.342(.031) | 57.4(2.4) |
| 32 | B | 6010(299) | 2.550(.260) | 2.006(.001) | 57.0(0.6) |
| 32 | C | 6110(198) | 2.950(.696) | 2.969(.002) | 57.6(0.3) |
| 32 | D | 6035(93) | 2.650(.464) | 3.892(.046) | 59.8(0.6) |
| 32 | E | 5450(320) | 2.025(.249) | 4.794(.006) | 62.4(0.7) |
| | | | | | |
| 100 mm Dia Support | | | | | |
| | Vel. | Damage Initiation | | Impact | Energy |
| Thick. | Code | Load | Energy | Velocity | Loss |
| (plies) | | (N) | (J) | (m/s) | (%) |
| | | | | | |
| 16 | A | 1785(65) | 2.100(.100) | 1.3279.004) | 67.0(3.5) |
| 16 | B | 1756(101) | 2.075(.083) | 2.004(.005) | 66.8(1.6) |
| 16 | C | 1825(25) | 2.250(.050) | 2.933(.010) | 46.8(0.8) |
| 16 | D | 1988(248) | 2.300(.224) | 3.896(.021) | 49.6(3.1) |
| 16 | E | 2005(137) | 2.267(.249) | 4.788(.008) | 52.1(3.0) |
| | | | | | |
| 32 | A | 5540(228) | 5.550(.150) | 1.330(.007) | 40.1(0.8) |
| 32 | B | 5525(192) | 5.700(.212) | 2.005(.003) | 43.6(0.6) |
| 32 | C | 5985(169) | 5.800(.141) | 2.921(.003) | 47.9(0.9) |
| 32 | D | 5680(328) | 5.600(.141) | 3.903(.018) | 47.4(1.1) |
| 32 | E | 5835(108) | 6.413(.288) | 4.759(.018) | 53.2(1.5) |
| | | | | | |

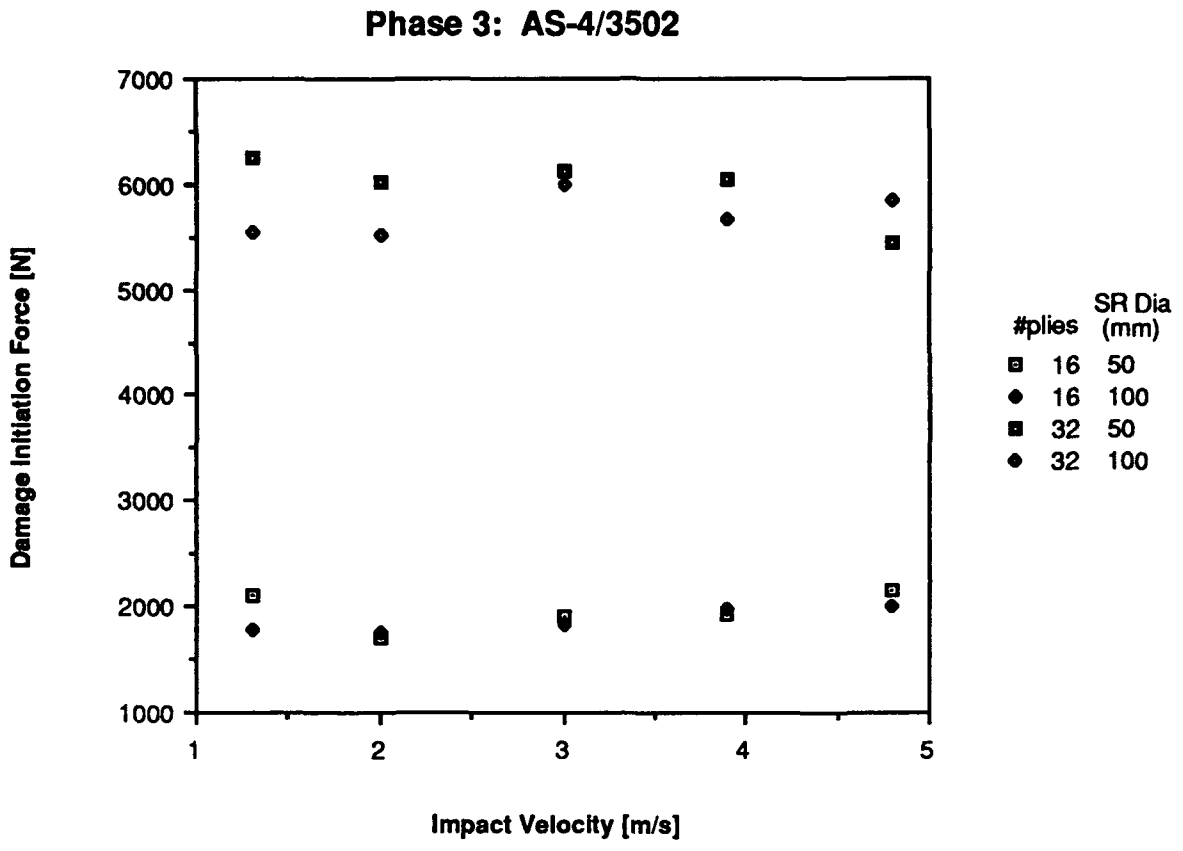


***Figure 4.13. Phase 3: AS-4/3502 data.***

Averaged Phase 3 data for the graphite/PEEK material are given in Table 4.10 and plotted in Figure 4.14. As with the graphite/epoxy material, the damage initiation force for the graphite/PEEK material is independent of the impact velocity in the low-velocity regime.

***Table 4.10 Phase 3: Averaged Graphite/PEEK Results.***

| 50 mm Dia. Support | | | | | |
|---|---|---|---|---|---|
| | Vel. | Damage | Initiation | Impact | Energy |
| Thick. (plies) | Code | Load (N) | Energy (J) | Velocity (m/s) | Loss (%) |
| 16 | A | 2567(81) | 2.000(.071) | 1.518(.010) | 62.3(1.4) |
| 16 | B | 2640(184) | 1.940(.014) | 2.357(.009) | 61.1(0.4) |
| 16 | C | 2490(N/A) | 1.935(N/A) | 3.461(.009) | 62.4(1.2) |
| 16 | D | 2740(184) | 2.350(.187) | 4.530(.008) | 59.3(0.2) |
| 32 | A | 6900(216) | 4.600(.141) | 1.513(.006) | 34.8(2.8) |
| 32 | B | 6100(283) | 4.250(.354) | 2.355(.010) | 43.4(1.8) |
| 32 | C | 6000(245) | 3.000(.367) | 3.461(.006) | 36.2(5.8) |
| 32 | D | 6020(107) | 3.750(.337) | 4.532(.017) | 32.2(0.9) |
| 100 mm Dia Support | | | | | |
| | Vel. | Damage | Initiation | Impact | Energy |
| Thick. (plies) | Code | Load (N) | Energy (J) | Velocity (m/s) | Loss (%) |
| 16 | A | 2863(114) | 4.180(.228) | 1.544(.005) | 49.8(3.4) |
| 16 | B | 2810(65) | 4.290(.085) | 2.365(.003) | 50.1(0.7) |
| 16 | C | 3075(25) | 4.305(.105) | 3.480(.004) | 24.2(0.1) |
| 16 | D | 3760(177) | N/A | 4.543(.023) | N/A |
| 32 | A | 6600(0) | 9.600(.000) | 1.468(.105) | 17.6(4.8) |
| 32 | B | 6750(50) | 9.870(.180) | 2.366(.009) | 21.6(0.4) |
| 32 | C | 6170(70) | 3.225(.525) | 3.477(.003) | 22.9(0.7) |
| 32 | D | 7150(50) | 9.765(.015) | 4.540(.037) | 20.5(1.8) |

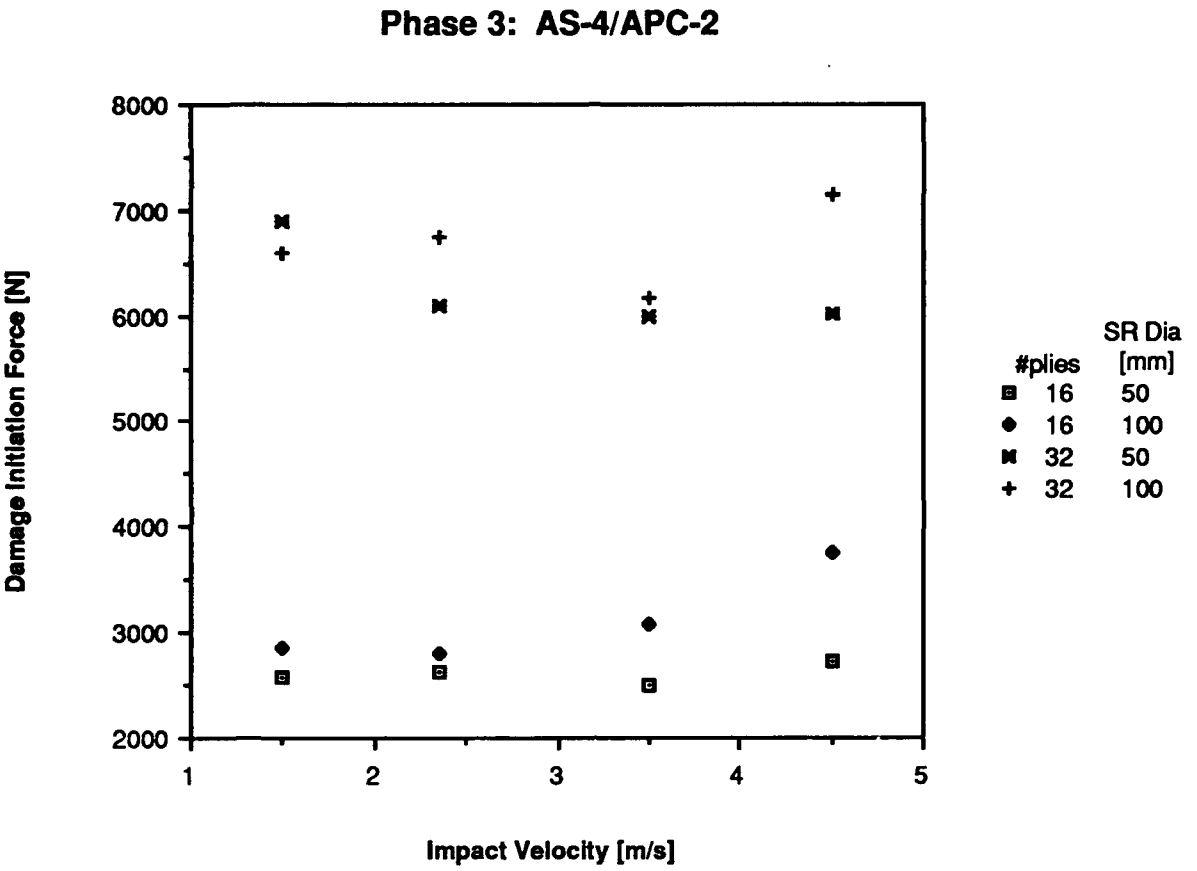


***Figure 4.14. Phase 3: AS-4/APC-2 data.***

## 4.3 Fractographic and Ultrasonic Inspection of Tested Specimens

Representative C-scans and photographs of exterior surfaces of impacted, graphite/epoxy and graphite/PEEK specimens are shown in Figures 4.15 and 4.16. Since the C-scans of the statically tested specimens were identical to those of the impacted the former are not shown in this report.

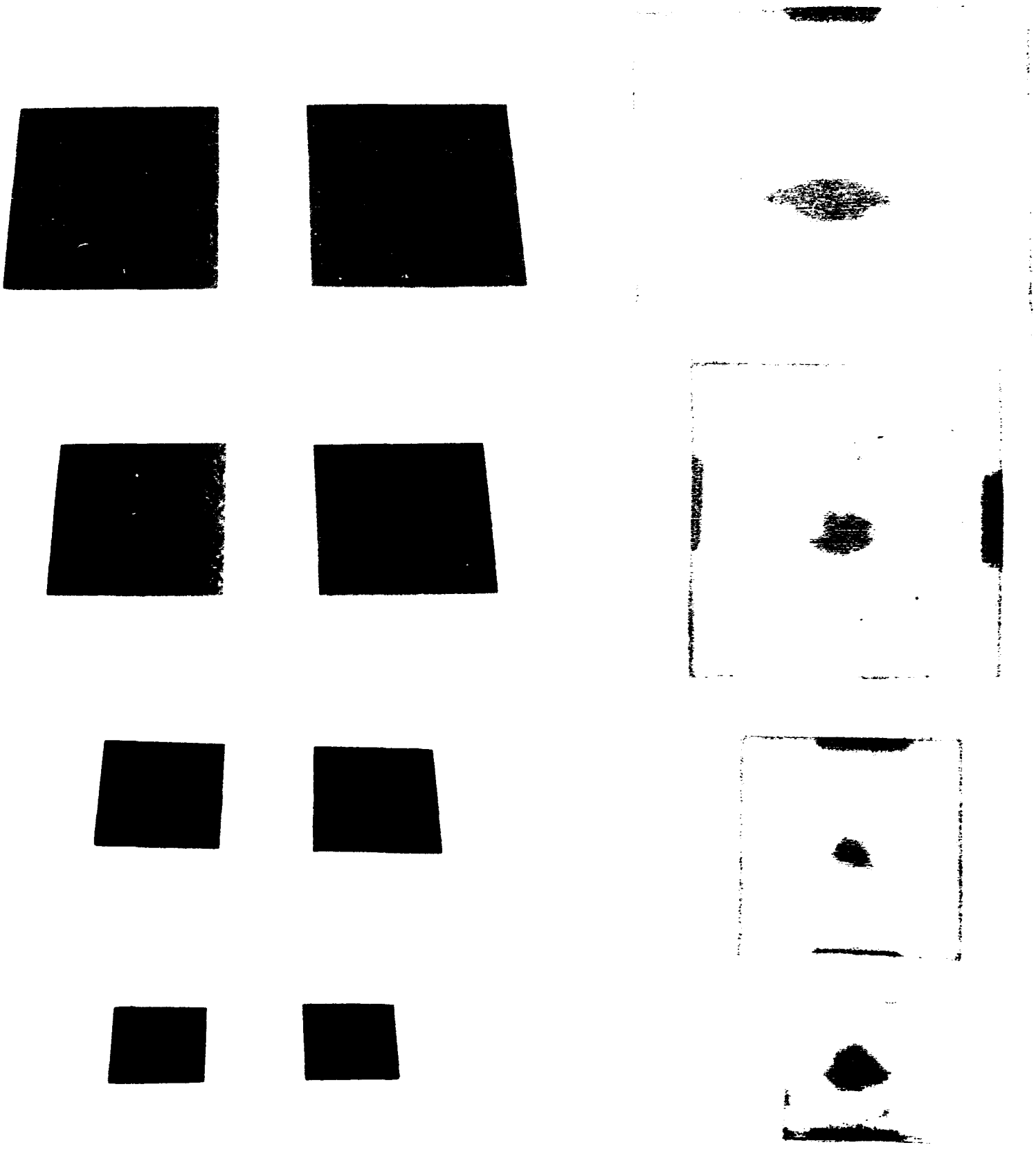

*Figure 4.15. Inspection of impacted graphite/epoxy specimens.*

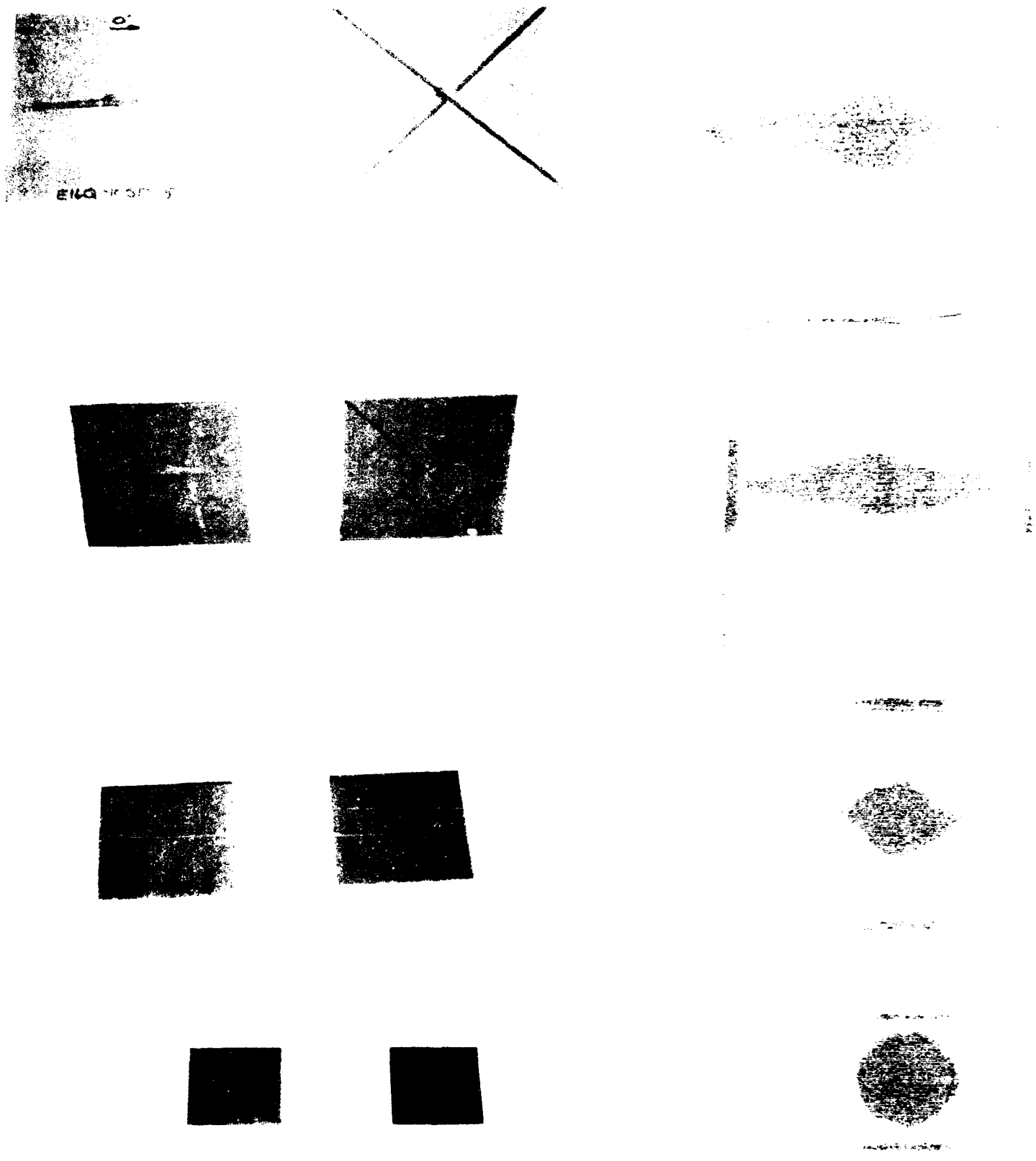

*Figure 4.16 Inspection of impacted graphite/PEEK specimens.*

Photomicrographs of representative impacted graphite/epoxy and graphite/PEEK specimens are given in Figures 4.17, 4.18 and 4.19. As with the C-scans, no significant difference was noted in the failure modes of the statically tested specimens versus the impacted specimens. Therefore, photomicrographs of the statically tested specimens are not presented in this report.

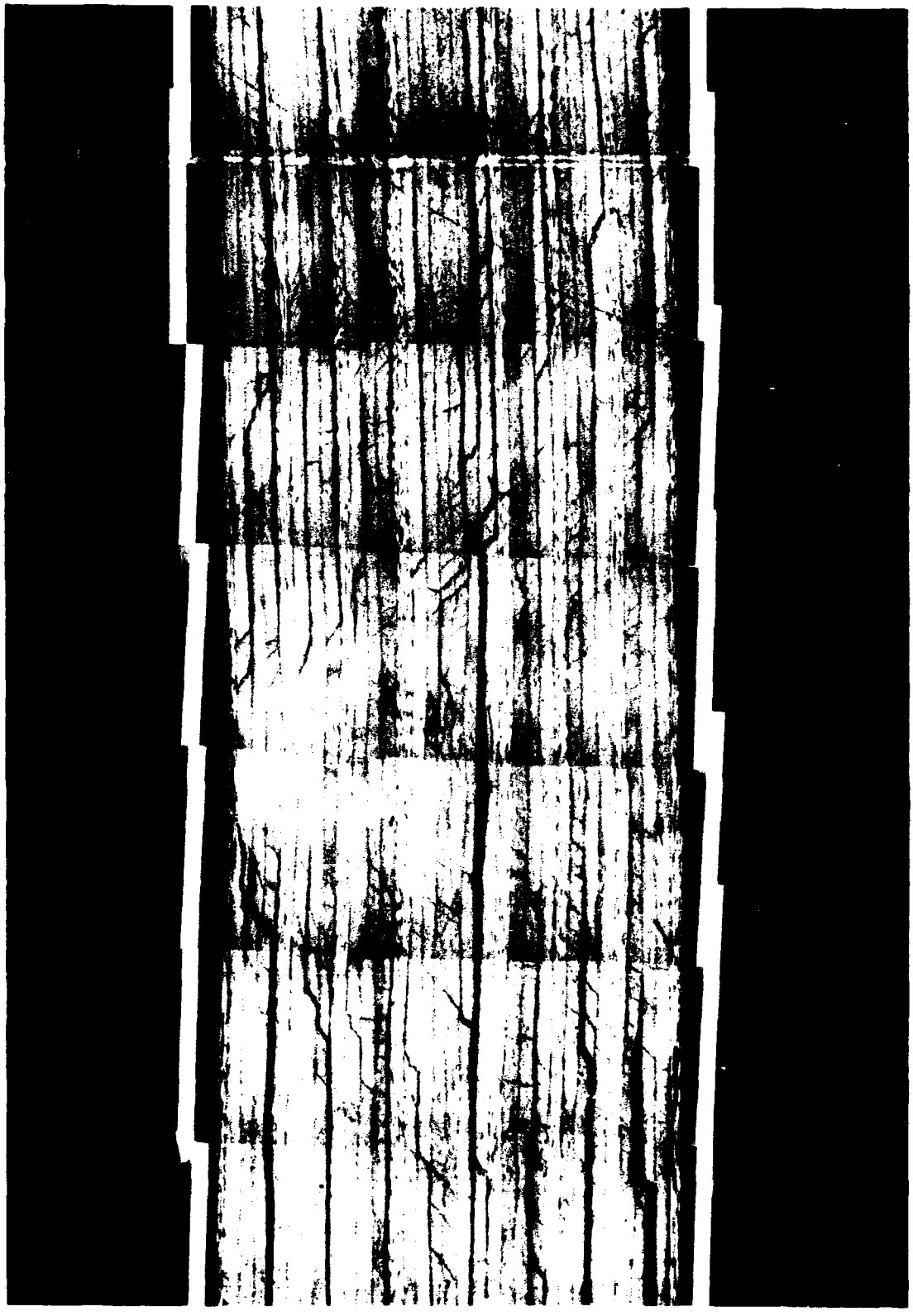

***Figure 4.17. Photomicrograph of impacted graphite/epoxy specimens.***

***Figure 4.18. Photomicrograph of impacted graphite/PEEK specimens showing no backface damage.***

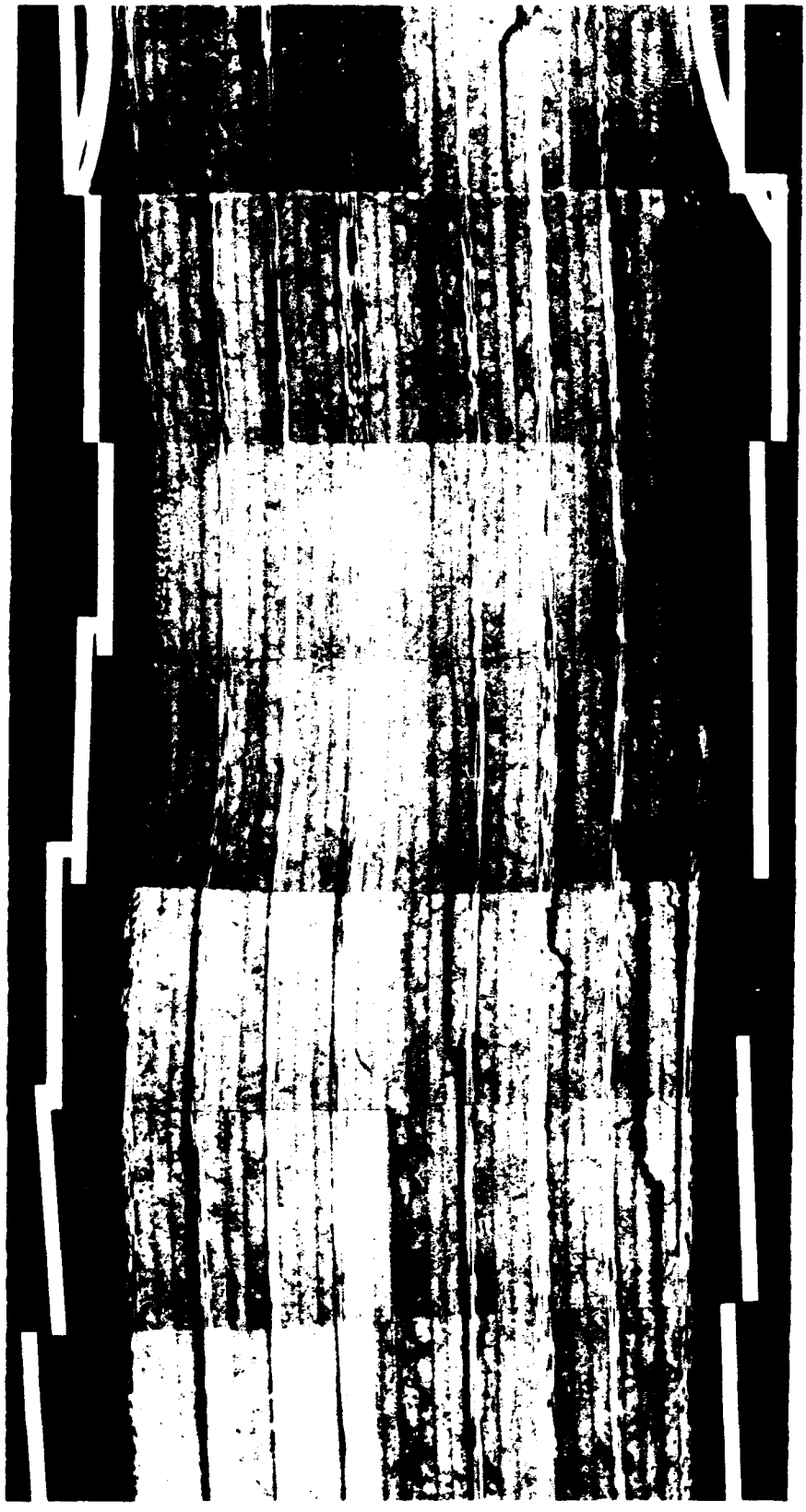

***Figure 4.19. Photomicrograph of impacted graphite/PEEK specimens showing backface damage.***

# SECTION 5. DISCUSSION

A comparison of the damage initiation force data obtained through static indentation and low-velocity impact indicates that there is not a significant difference in the data obtained for the two loading rates. This implies that the initial assumption of approximately static loading which justifies the application of the Hertz Contact Law in the derivation of the theoretical model is valid. However, since only two specimens were tested for each static test condition, the data obtained from the static tests may not be a good statistical representation. Therefore, it is recommended that more static indentation tests be conducted before any definitive conclusions are made concerning the effect of the loading rate on the damage initiation force.

For both materials, the Phase 1 data indicate that the damage initiation force is essentially independent of the specimen support size. This result is very desirable because it implies that low-velocity impact data can be generated using very small test specimens, and these data will be applicable to larger structures. This will save the material tester the cost associated with testing large structures and will allow for testing of experimental materials available in very limited quantities. Results of Phase 1 further show that damage initiation force data correspond rather well with the trend predicted by the theoretical model. This, however is not the case for the Phase 2 data. The theoretical model predicts the damage initiation force to be proportional to the square root of the indenter nose diameter. The Phase 2 experimental data showed the damage initiation force to be a function of the indenter nose diameter raised to the 0.25 power. The exact reasons for the inconsistency between theoretical predictions and experimental data are not clear at this time. One possible explanation may be related to the fact that the theoretical model assumes that the composite will fail solely by shear. Photomicrographs indicate a slightly more complex failure mode. A statistical analysis of the Phase 2 experimental data indicates that it is likely that there is an interaction effect between the indenter nose diameter, material thickness, and specimen support size for both materials. From this, it can be concluded that the damage initiation force is independent of the specimen support size for a given indenter nose diameter. Phase 3 data reveal the damage initiation force to be essentially independent of the velocity at impact, for impact velocities less than 5 m/s. This result allows the operator to test at a greater number of energy test levels since the operator will not be constrained by having to keep the impact velocity (impacter drop height) at the same level throughout the entire investigation.

Inspection of the back surfaces of the impacted laminates indicates significant difference in the types of failure of the two materials. Damage on the impacted side of the thermoplastic matrix specimens (graphite/PEEK) generally appeared as a round dent surrounded by one or two small transverse cracks. These cracks consist of buckled surface fibers which are believed to occur because of very high compressive stresses in the immediate neighborhood of the impact site. The damage area on the backface of the laminates was relatively small. C-scans showed localized oval shaped damage. The thermoset matrix specimens (graphite/epoxy) failed in a more brittle manner and had significant backface damage and fiber breakage. Ultrasonic inspection shows the damage to extend the length of the specimen support and to occur in the direction of the outer ply fibers.

The predominant failure mode for the thermoset matrix material was found to be delamination. The delaminations appeared to originate from matrix shear cracks which initiated under the indenter nose and propagated through the thickness in a conical fashion. The result was extensive damage on the backface of the laminate. The matrix shear cracks and backface damage became less apparent as the thickness of the material increased, while delaminations became more apparent. This observation indicates that it is likely that delaminations occur before backface damage for the graphite/epoxy material. This type of failure mode is associated with failure resulting from contact forces.

Examination of the photomicrographs of the tested graphite/PEEK specimens showed two predominant failure modes which appear to be thickness dependent. Since the 32-ply specimens exhibit both modes of failure, it is suggested that 32 plies is close to the critical thickness for which a change of failure modes occurs. For the thinner specimens as well as some of the 32-ply specimens, the photomicrographs indicate a mode of failure which is predominantly backface damage with some delamination and matrix cracking. A small amount of plastic deformation was visible on the impacted side of the laminate. The amount of delamination occurring in the thermoplastic matrix test specimens decreased with increasing specimen thickness for the range of thicknesses examined. From the photos, it can be concluded that for the thinner graphite/PEEK specimens it is likely that backface damage occurs before delamination. This type of failure is characteristic of the failure associated with flexural deformation of the specimen during impact. This flexural type of failure can be attributed to the higher strain to failure of the thermoplastic material and the thickness of the specimens tested. As mentioned previously, a second failure mode was apparent for the 32 ply, graphite/PEEK specimens impacted under identical test conditions.

This mode of failure was similar to that noted for the graphite/epoxy specimens in which delaminations originated from matrix shear cracks. The matrix shear cracks were found to initiate under the indenter nose and to propagate through the thickness in a conical fashion. No backface damage was found to accompany the delaminations. As with the thermoset matrix material, this type of failure mode is attributed to contact forces rather than to flexural deformation of the test specimen.

From the discussion above, it can be concluded that the failure mode which composites exhibit when subjected to low-velocity impacts is dependent on two parameters: material thickness and material toughness. For thick and/or brittle materials such as the graphite/epoxy or 32-ply, graphite/PEEK specimens, the failure results from contact forces and is dominated by interlaminar failure. For thin and/or ductile materials such as the thin, graphite/PEEK specimens, the failure results from flexural deformation of the test specimen and is governed by backface tensile failure of the fibers.

# SECTION 6. CONCLUSIONS

1. No significant difference was found between the static indentation tests and the low-velocity impact tests. This validates the initial assumption of approximately static loading which allows for the application of the Hertz contact law. However, since only a few specimens were tested for each static indentation test condition, a meaningful statistical analysis could not be conducted comparing the static vs low-velocity results. Therefore, more investigation is needed to statistically verify this result.

2. The damage initiation force is essentially independent of specimen support size for a given indenter nose diameter.

3. The damage initiation force can be described by the following empirical relation:

$$P = C\, h^{1.5}\, D^{0.25} \tag{6.1}$$

4. The damage initiation force is essentially independent of impact velocity.

5. The damage area for the graphite/epoxy material is much greater than that of the graphite/PEEK. The mode of failure which composites exhibit when subjected to low-velocity impacts is dependent on both material thickness and material toughness. For thick and/or brittle materials such as the graphite/epoxy or 32-ply, graphite/PEEK specimens, the failure results from contact forces and is dominated by interlaminar failure and matrix cracking. For thin and/or ductile materials such as the thin, graphite/PEEK specimens, the failure results from flexural deformation in which tensile failure of the fibers occurs on the backface of the specimen.

# REFERENCES

[1] Cordell, T. and Sjöblom, P., "Low-Velocity Impact Testing of Composites," Proceedings of the American Society for Composites, First Technical Conference, pp. 297-312, Dayton, OH, 7-9 October 1986.

[2] Kitanka, M., Kobayaski, H., Norita, T. and Kawatsu, Y., "Damage Tolerance of Thermoplastic/Graphite Fiber Composites." Proceedings of the Fifth International Conference on Composite Materials, p. 913, San Diego, CA., 1985.

[3] Cantwell, W. and Morton, J., "Detection of Impact Damage in CFRP Laminates," Composite Structures, Elsevier Applied Science Publishers, Amsterdam, 1986, pp. 251-260.

[4] Sjöblom, P., "Simple Design Approach Against Low-Velocity Impact Damage," 32nd International SAMPE Symposium and Exhibition, pp. 529-539, Anaheim, CA, 6-9 April 1987.

[5] Yang, S. and Sun, C., "Indentation Law for Composites," ASTM STP 563, 1974.



☆U.S. GOVERNMENT PRINTING OFFICE: 1991 - 548-076/44273